Seasonal Temperature and Stress Distributions in Concrete Gravity Dams

by

John Venturelli

Department of Civil Engineering

and Applied Mechanics

McGill University

Montréal, Québec

June 1992

A thesis submitted to the Faculty of Graduate Studies and Research in partial fulfilment of the requirements for the degree of Master of Engineering.

Abstract

Seasonal thermal stresses have been found to contribute significantly to the long term degradation of strength and stiffness of concrete dams located in northern regions. Moreover, thermal stresses and strains must be evaluated to define the initial loading conditions for seismic safety analyses. In this study, finite element procedures to model the thermal response of concrete gravity dams are presented. Heat transfer and structural models of a typical dam-foundation-reservoir system are developed. The reservoir, foundation, and air temperature variations, as well as solar radiation, are evaluated from data collected from different sources. The rate of convergence of the numerical solution is examined, and a methodology to identify the critical temperature states and to compute the related stresses, considering creep, is presented.

Extensive parametric analyses are then performed to determine the relative influence of (i) the geometrical, thermal, and mechanical properties of the dam, (ii) the reservoir, foundation and air temperature distributions, and (iii) the heat supply from solar radiation, on the stress-strain response of the system. Temperature states to define critical stress conditions for structural safety analysis are determined.

Significant thermal stresses occur in the vicinity of the exposed surfaces of the dam. The typical depth of frost penetration is about 6m. The parameters which affect the surface stresses most are the air temperature distribution and the height of the dam, while for the frost penetration they are the solar radiation, convection coefficient, and conduction coefficient.

Résumé

Les contraintes saisonnières d'origine thermique contribuent de façon significative à la dégradation de la rigidité et de la résistance des barrages de béton situés en régions nordiques. De plus, les contraintes et déformations d'origine thermique doivent être évaluées afin de définir les conditions initiales pour les analyses de vérification sismiques. Dans cette étude, une procédure utilisant la méthode des éléments finis pour modéliser la réponse thermique des barrage-poids en béton est présentée. Des modèles d'analyse de transfert de chaleur et structural sont développés pour un système barrage-fondation-réservoir typique. Les variations de températures du réservoir, de la fondation et de l'air, de même que l'effet des radiations solaire sont évaluées à partir de données obtenues de différentes sources. La convergence des solutions numériques est examinée, et une méthodologie pour identifier les états critiques de température et calculer les contraintes qui y sont associées, tout en tenant compte du fluage, est présentée.

Une étude paramétrique exhaustive est menée afin de déterminer l'influence (i) des propriétés géométriques, thermiques, et mécaniques du barrage, (ii) de la distribution des températures dans le réservoir, la fondation, et l'air, et (iii) de l'absorption de chaleur par radiation solaire, sur l'état de contrainte et de déformation du système. Les distributions critiques de température définissant les conditions initiales pour des études d'intégrité structurale subséquentes sont établies.

Des contraintes thermiques importantes se produisent près des surfaces exposées du barrage. La pénétration typique du gel et d'environ 6m. Les paramètres qui affectent le plus les contraintes de surface sont la température de l'air et la hauteur du barrage, alors que pour la

pénétration du gel ce sont les radiations solaire, le coefficient de conduction, et le coefficient de convection.

Acknowledgements

The author would like to express his gratitude to his research supervisor, Dr. P. Léger, for the helpful comments and suggestions made during the course of this study.

The financial support provided by the F.O. Fowler Fellowship was greatly appreciated. The computational environment provided by research funds from the National Sciences and Engineering Research Council of Canada is gratefully acknowledged.

The author would like to thank Sudip Bhattacharjee for his assistance in verifying the computational results, and Eduardo Guevara for having helped in preparing the computer models.

Table of Contents

List of Figures

List of Tables

CHAPTER 1

Introduction

1.1 Overview and Objectives

The safety evaluation of concrete dams is a complex problem due to the uncertainties related to the prediction of the spatial and temporal variations of applied loadings such as temperature, ice, and earthquakes. Moreover, long term aging of the dam-foundation system is characterized by a decrease in stiffness and resistance over time, as evidenced by concrete cracking observed in several dams (Fig. 1.1). The time degradation of mechanical properties can be significantly accelerated in the presence of alkali-aggregate reactions, water aggressivity, freezing and thawing, and foundation differential settlement.

In northern regions, like the province of Quebec, thermally induced cyclic stresses have been shown to play a significant role in the degradation of the strength and stiffness of concrete dams (Ballivy et al. 1991; Veltrop et al. 1990; Tahmazian et al. 1989). Thermal stresses must therefore be considered in the structural safety evaluation procedures. A report on deterioration of dams and reservoirs published by ICOLD (1984) lists freezing and thawing, and external temperature variations, to be the most common cause of deterioration in concrete dams. As can be seen from Table 1.1, seasonal temperature cycles and variations are the cause of deterioration

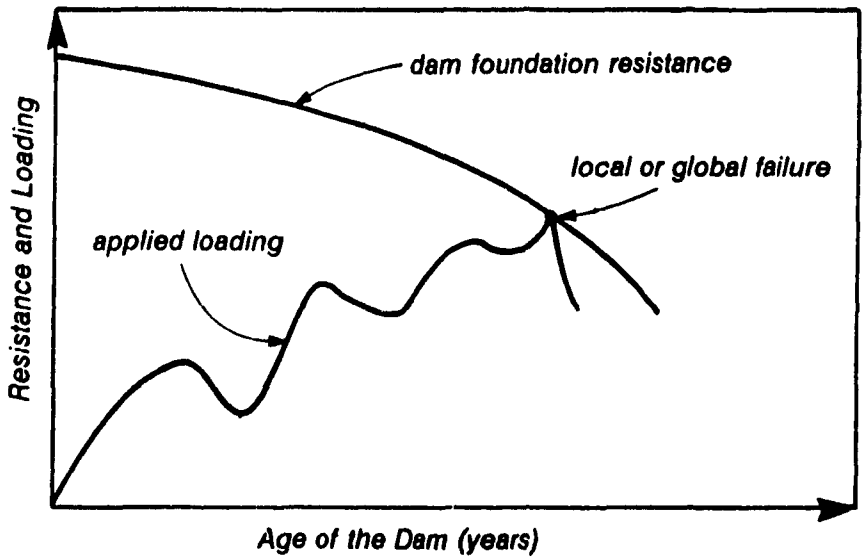

Figure 1.1 Time variation of structural resistance and applied loading (adapted from Jacobs, 1988).

in 28% of cases.

The recent earthquake activities in Quebec have raised serious questions regarding the seismic vulnerability of critical aging structures such as concrete dams, and a knowledge of thermal stresses is required to perform a thorough safety evaluation (Dascal 1991; 1990). Figure 1.2 indicates the location of the main concrete dams (above 25m) in Quebec, the yearly normal freezing index in degree days (°C), that is defined as the cumulative total of the difference between daily mean air temperatures and the freezing point, and the epicentre location of the 1988 Saguenay earthquake, that contained high energy in the frequency range of concrete dams. To investigate the seismic safety of concrete dams, it is essential to quantify the static state of stress and strain that exists at the time the earthquake occurs. The pre-earthquake initial stress and strain distributions are primarily due to gravity loads and hydrostatic pressure. Thermal, shrinkage, and creep strains may also have a major effect on the initial condition in which the earthquake finds the dam. The temperature gradient through old dams is controlled by the cyclic

Table 1.1 Most frequent classification headings of deterioration for concrete dams (ICOLD 1984)

Classification Heading of Deterioration	Percentage of Dams Affected
1. Resistance to freezing and thawing	19
2 External temperature variations	9
3. Permeability	9
4 Reactions between concrete constituents and environment	8
5 Concreting	7
6. Percolation (foundation)	6
7 Temp. variations due to heat of hydration	6
8. Reactions of concrete constituents	6
9. Structural joints	5
10. Uplift (foundation or dam body)	5
11. Internal erosion	5
12 Deformation and land subsidence	3
13 Tensile stresses	3
14. Grout curtains and other watertight systems	2
15 Drainage systems	2
16. Cleaning of drains	2

seasonal temperature and climatic variations. The strain capacity available to resist the seismic induced forces without concrete damage will thus be affected to a different degree depending on the season in which the seismic event may occur. For a given earthquake, several analyses might therefore be required to consider the initial conditions at different times during the expected service life of the dam (NRC 1990).

The objective of this study is to develop a methodology to evaluate the thermal stresses

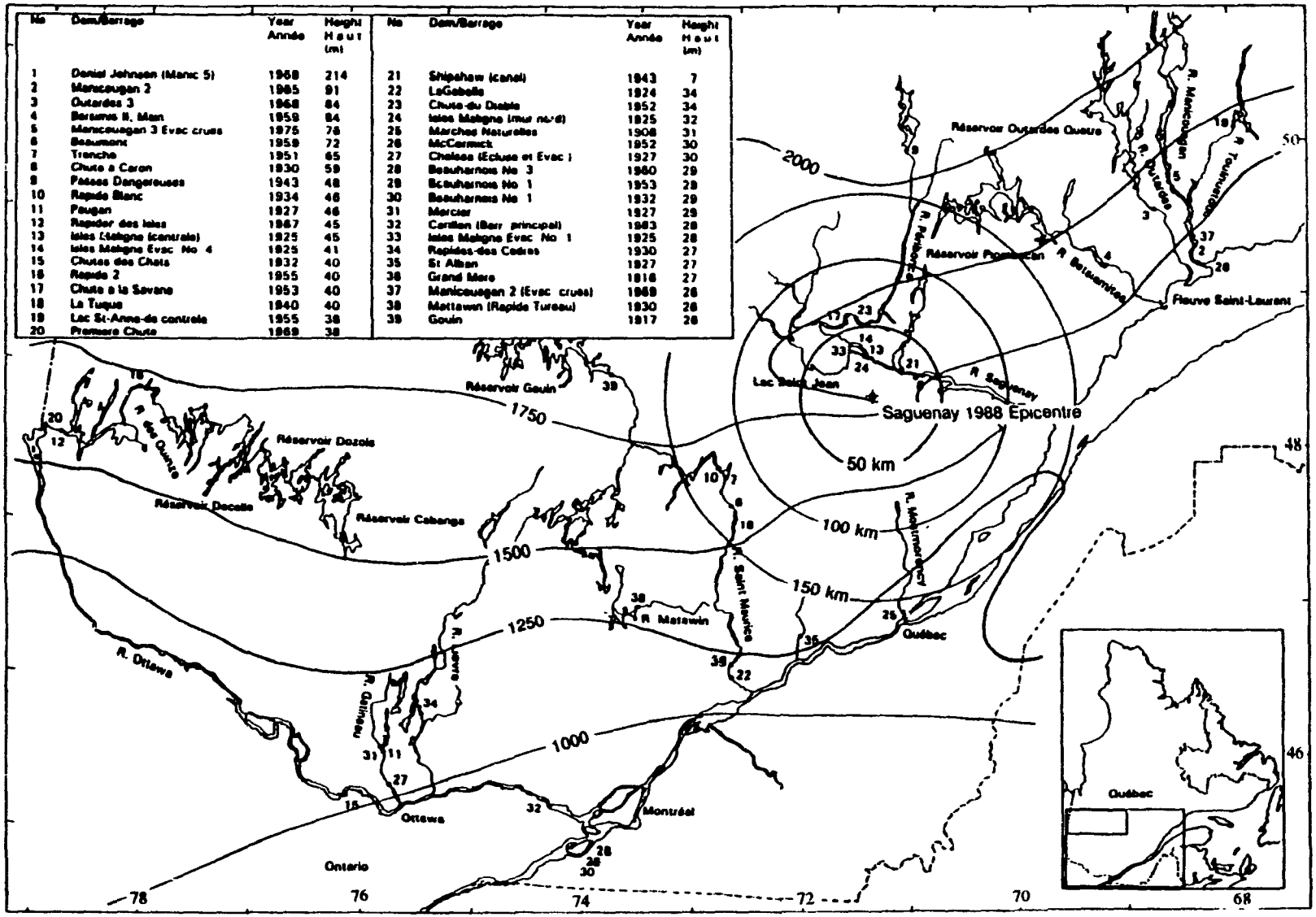

Figure 1.2 Location of major concrete dams in Quebec, the freezing index, and 1988 Saguenay earthquake.

and strains in typical concrete gravity dams located in northern regions. Finite element models suitable for transient heat transfer and subsequent structural analyses are presented. The reservoir, foundation, and air temperature distributions, the heat supply from solar radiation, and the geometrical, thermal, and mechanical properties of typical dam foundation reservoir systems are developed from data collected from various sources. The numerical convergence of transient heat flow analyses is examined. The initial temperature distribution, the reference thermal state to compute seasonal stress oscillations, and a methodology to determine critical temperature distributions for structural safety investigations are presented.

1.2 Past Work

Many empirical methods and closed form solutions exist to obtain the thermal distribution in dams. But the reliability of these methods as environmental conditions vary from site to site are not known. The finite differences method (Schimdt method) has also been used to obtain thermal distributions. Figure 1.3 shows the temperature field obtained by this method for Oust-Illim gravity dam (USSR) during operational conditions (Rosanov et al. 1970). Actual measurements of dam temperatures may also be used to obtain thermal stresses, as was done at Fontana dam, but this is not a practical approach (142 m, North Carolina, USA; Fig 1.4; Baylosis 1988). The finite element method (FEM) has been recently used to conduct transient heat flow analysis. Veltrop et al. have used the FEM to obtain the temperature distribution at Daniel Johnson multiple arch dam (214m, Quebec, Canada), which was experiencing thermal cracking. Their analysis was based on a sinusoidal representation of air and reservoir temperature. Paul and Tarbox (1991) have presented a finite element analysis of the temperature and stress distribution in arch dams. A more detailed review of previous contributions to the

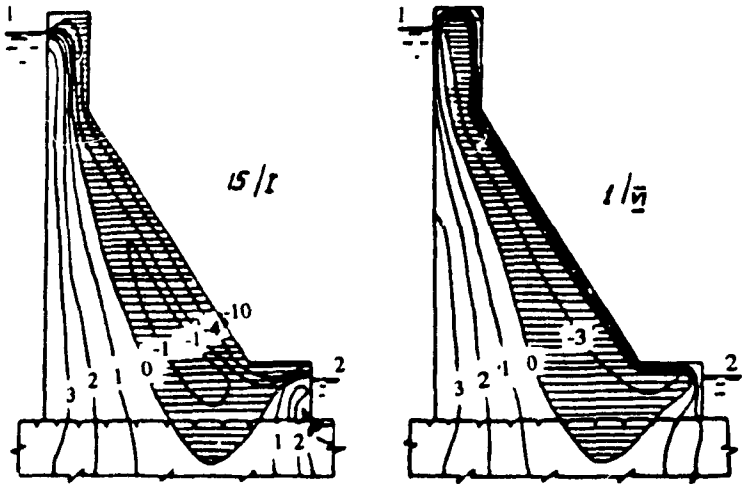

Figure 1.3 Temperature field of a massive gravity dam in operation, in °C (Oust-Illim dam, USSR; Rosanov et al. 1970).

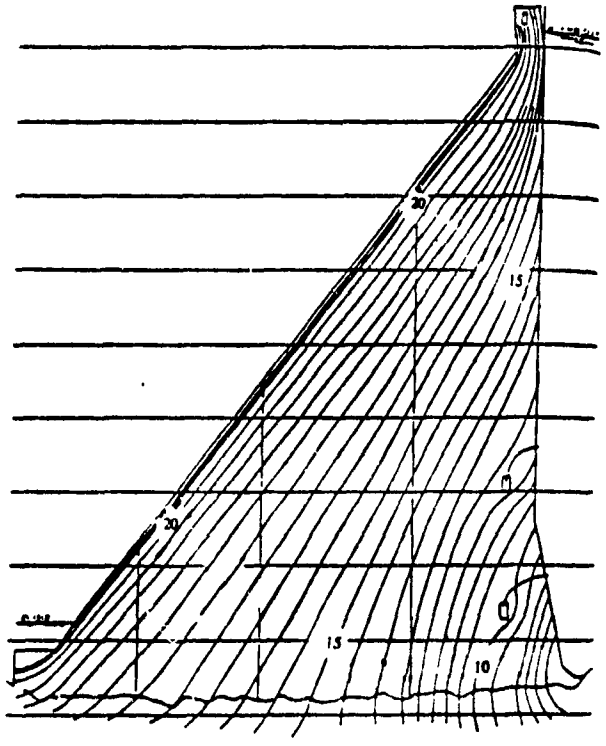

Figure 1.4 Mean annual temperature for Fontana dam, in °C (Baylosis 1988).

thermo-mechanical analysis of dam-foundation-reservoir systems is presented in chapter 2.

1.3 Organization of the Thesis

Chapter 2 presents a review of the heat transfer process, the structural modelling procedures, and the computational procedures. In Chapter 3 the transient heat flow analysis using the FEM is explained in detail. Chapter 4 introduces the dam- foundation-reservoir model used in the preliminary analysis.

In Chapter 5 the procedure to define the environmental parameters affecting the thermal response are explained. In Chapter 6 convergence of the heat transfer analysis, and the preliminary results on temperature and stress distributions, are introduced. An extensive parametric analysis is then performed in Chapter 7 to determine the influence of different modelling parameters, related to the geometry, mechanical and thermal properties, and environmental parameters, on the computed temperature and stress distribution. Finally, in Chapter 8 a summary, conclusions, and future research directions are presented.

CHAPTER 2

Structural Analysis of Concrete Dams Including Thermal Effects

2.1 Heat Transfer Processes and Thermal Stresses

Figure 2.1a summarizes the main sources of internal and external loads that might contribute to the cracking of concrete gravity dams. The internal thermal load consists in the hydration heat, while the external thermal loads are produced by solar radiation, air, reservoir, and foundation temperatures. Frost, snow, and ice covers will also affect the thermal response of the dam-foundation-reservoir system. Figure 2.1b describes the heat transfer processes occurring in a dam-foundation-reservoir system and the thermal boundary conditions adopted in this study. These temperature fluctuations produce volumetric changes of the dam. If these volumetric changes are restrained, temperature stresses will develop. The restraints may be caused by internal or external conditions. Internal restraints are induced by a difference in temperature between the interior and the exterior of the dam. External restraints are provided by the stiffness of the restraining foundation, and the three-dimensional interaction between adjacent monoliths, as shown in Fig. 2.2.

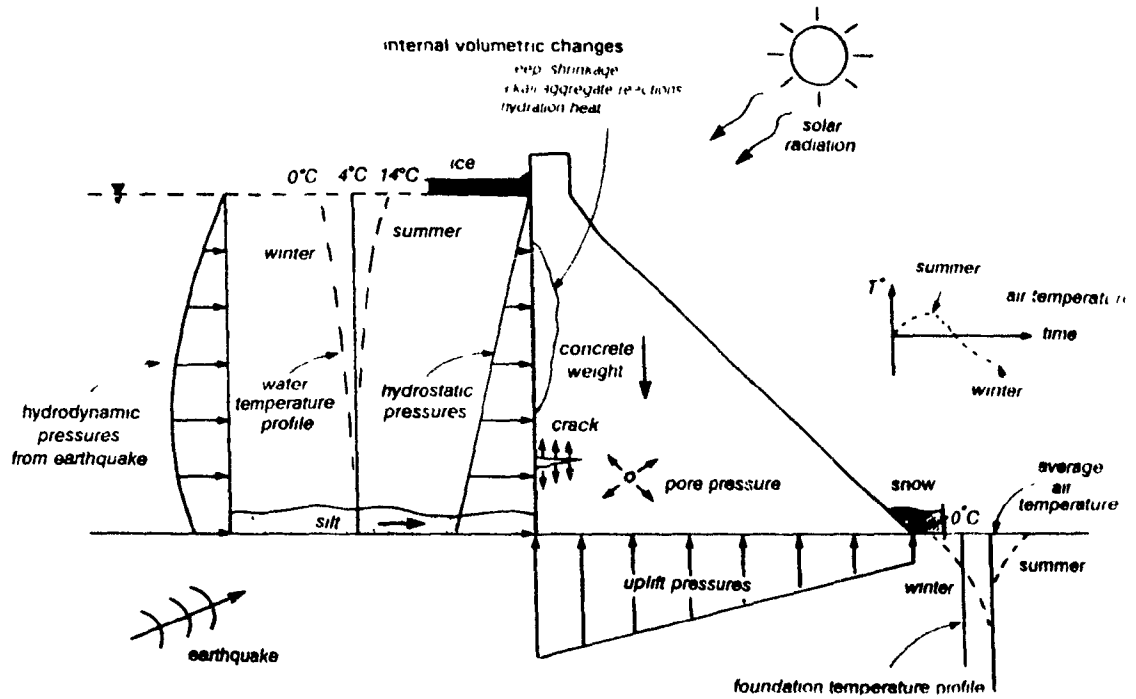

(a)

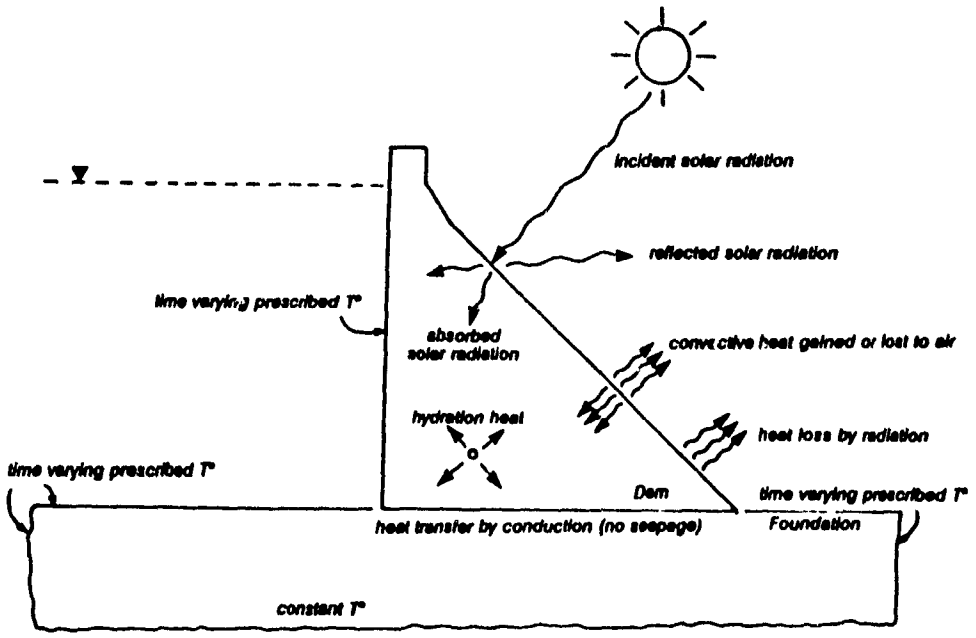

(b)

Figure 2.1 Loading on concrete dams: (a) static, thermal, and dynamic loads; (b) heat transfer processes for dam.

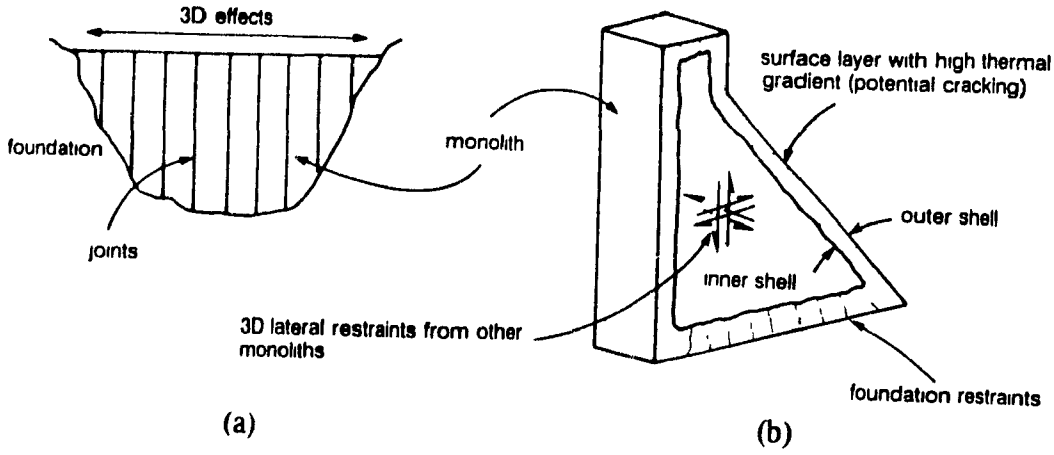

Figure 2.2 Restraints to volumetric changes: (a) dam-foundation; (b) individual monolith.

2.2 Computational Procedures

Internal temperature stresses are induced during the incremental construction process. These residual stresses involve a complex nonlinear interaction of creep, shrinkage, and thermal effects of young mass concrete that are difficult to predict either experimentally or numerically (Truman et al. 1991a,b; Sadouki and Wittmann 1991; Ishikawa 1991; Machida and Uehara 1987). Cracking provides a stress relief mechanism for internal residual tensile stresses exceeding the tensile strength of the concrete. These cracks affect the structural behaviour of the dam only if they allow water penetration and/or are located in areas where operational loads induce tensile stresses (Widmann 1990).

Temperature observations in many dams have indicated that after the construction phase is past, a regular periodic change in the temperature of the dam will gradually appear (Fig. 2.3; Tarbox 1977; Baylosis 1988). In large dams, a natural balance or "temperature stability" will be established between the internal and external temperatures after many years. The

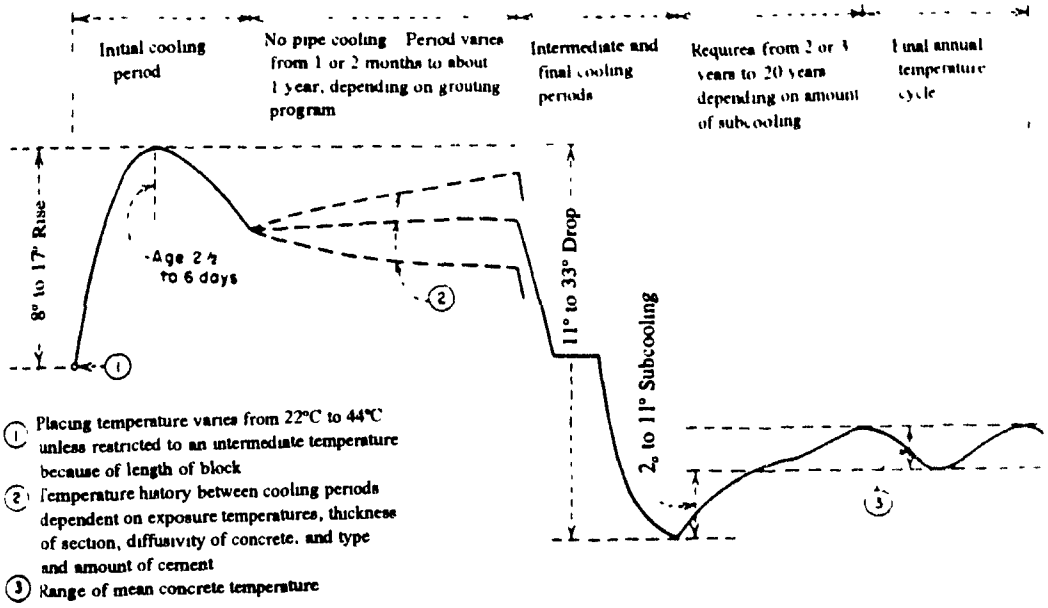

Figure 2.3 Temperature history of artificially cooled concrete (Tarbox 1977).

"temperature stability" has been defined by Baylosis (1988) as the "condition where radical temperature changes will no longer occur to cause large movements in the dam or high stresses, except in the zone immediately adjacent to the faces". Detailed experimental and numerical investigations of the thermal response of Fontana gravity dam (142 m, North Carolina, USA) and Daniel Johnson multiple arch dam have indicated that the "temperature stability", or reference temperature state, upon which seasonal variations will oscillate, is approximately equal to the long term mean air temperature at the site (Paul and Tarbox 1991; Baylosis 1988).

The seasonal thermal oscillations effects can be included in the structural analysis using different modelling techniques (Cervera et al. 1990):

(i) A coupled time advancing thermo-elastic or thermo-inelastic problem dealing simultaneously with displacements and temperatures can be performed. Material modelling can include

temperature dependence of all parameters, anisotropic thermal conductivity, and gap conductance and radiation. Allowance for water and air penetration through cracks, with related conductivity across the cracks and cross radiation as a function of crack width, should be ideally considered (Norman and Anderson 1985). This alternative is numerically very expensive and requires detailed information about the three-dimensional thermal history of the concrete surfaces that is generally not available.

(ii) A separate thermal analysis can be performed to define critical temperature distributions that can be used subsequently as input for the structural analysis model. The thermal analysis can be performed with different degree of sophistication. Simple assumptions of structural restraints (eg. semi-infinite solid) and sinusoidal variations of thermal boundary conditions will lead to closed form analytical solutions to approximate the temperature gradients within the cross-section (Geinats et al. 1989; ACI 1981; Leliavsky 1981; USBR 1977). Finite differences (Schmidt method) has also been used extensively to deal with more complex variations of the applied temperature field. Alternatively, transient or steady-state heat flow analysis using the Finite Element Method (FEM) can be carried out (Paul and Tarbox 1991; Fanelli and Giuseppetti 1985; Tarbox 1977). The FEM can be used effectively to determine the temperature distribution in a structure with complex geometry and boundary conditions. The same model can be utilized for heat transfer and stress analyses, therefore minimizing the required effort to generate the input data.

(iii) If extensive measured internal and external temperature field data exists, these can be interpolated directly to define the isothermal contours at different times of the year.

2.3 Structural Models

Concrete gravity dams are generally analyzed using two-dimensional models. To establish the initial conditions a plane-stress or a plane-strain idealization may be adopted depending on the degree of restraint provided by the presence of vertical joints between the monoliths. Three-dimensional analysis should be considered for dams located in relatively narrow valleys, with crest-length-to-height ratios of 5 to 1 or less, or having irregular shapes from one abutment to another (NRC 1990). Thermal strains can induce longitudinal and related frictional forces perpendicular to the contraction joints that will produce significant three-dimensional load carrying mechanisms, causing the dam to behave more like a continuous structure. The tightening of the contraction joints will alter the static (ie., stiffness) and dynamic (ie.,natural periods, damping level) properties of the dam. Variations of ambient temperature have also been found to affect the effectiveness of the grout curtain of concrete dams (Kalkani 1992).

CHAPTER 3

Heat Transfer Analysis

3.1 Heat Flow Equilibrium Equation

The structural and thermal behaviour of typical concrete gravity dams can be represented by two-dimensional models assuming a uniform distribution of the thermal properties and boundary conditions along the longitudinal axis.

In two dimensions the transient heat conduction equation for an isotropic material defined in the x-y plane is:

[3.1] $$\frac{\partial^2 T}{\partial x^2} + \frac{\partial^2 T}{\partial y^2} + \frac{q}{k} = \frac{\rho c}{k} \frac{\partial T}{\partial t}$$

in which T is the temperature of the medium, in °K; k is the isotropic thermal conductivity coefficient, in W/(m °K); q is the heat generated within the body (eg. by hydration), in W/m^3; ρ is the density, in kg/m^3; c is the specific heat, in J/(kg °K); t is the time, in seconds.

The matrix equation for heat flow equilibrium can be derived for the unknown temperatures, {T(t)}, at each node of the finite element model as (Cook et al. 1989):

[3.2] $$[C]\{\dot{T}(t)\} + [K]\{T(t)\} = \{Q(t)\}$$

in which [C] is the system heat capacity matrix which is dependent on ρ and c; [K] is the system thermal conductivity matrix. The system heat flux vector, {Q(t)}, can be written as

$$\{Q(t)\} = \{Q(t)\}_e + \{Q(t)\}_c + \{Q(t)\}_r + \{Q(t)\}_i \qquad [3.3]$$

where $\{Q(t)\}_e$ is the externally supplied heat flux; $\{Q(t)\}_c$ is the convective heat transfer at the surfaces; $\{Q(t)\}_r$ is the radiative heat transfer at the surfaces; $\{Q(t)\}_i$ is the internal heat generation (eg. from hydration). In absence of any radiation, {Q(t)} can be formulated independently of the unknown temperatures. The system of heat transfer equations is then linear and can be solved directly by a step-by-step integration procedure. The presence of radiating boundary conditions induces nonlinearity in the analysis such that the solution at each time step must be found by iteration (Bathe 1982). This increases very significantly the required computational effort.

If water is present in the concrete and it goes through a phase change, the internal heat transfer process will be affected. Before water can change phase from liquid to solid (or solid to liquid) it must release (or gain) a certain amount of energy. This energy is the latent heat of fusion, which for pure water is 334 J/g. In the thermal analysis of soil with a high water content, the phase change process has been found to have a significant impact on the depth of frost penetration. Considering the low permeability of concrete, the effect of water changing phase as the frost line moves from the downstream face towards the upstream face was not considered in the study.

3.2 Thermal Boundary Conditions

To determine a unique solution to the heat transfer equations, the initial temperature distribution throughout the system at time zero must be defined, and the thermal boundary conditions at the concrete-air, concrete-water, and concrete-foundation interfaces must also be specified.

3.2.1 Concrete-Air Interface

The heat transfer between the dam and the air boundary layer is a function of air and concrete temperature, wind speed, and solar radiation intensity. For a dam in normal operating condition, the downstream face receives a significant amount of radiant heat from the sun. This will cause the temperature of the concrete surface to be above that of the surrounding air. Therefore, the following boundary conditions must be considered at the concrete-air interface; (i) heat flow from the sun, (ii) convection, and (iii) radiation. The amount of solar energy, I_t (W/m^2), that is absorbed by the dam is given by:

[3.4]
$$q_s = a\, I_t$$

in which a is the solar absorptivity of the surface.

The heat gained or lost to the surrounding air as a result of temperature differences between the dam surface and the air is due to convection and is given by Newton's law of cooling:

[3.5] $$q_c = -h_c(T_a - T)$$

in which h_c is the convection coefficient, in W/(m²°K); T is the temperature of the surface, in °K; T_a is the temperature of the surrounding air, in °K. The surface temperature of a dam subjected to convection heat transfer will generally follow closely the air temperature variation. The amount by which the surface temperature lags behind the air temperature depends on the convection coefficient. If a large convection coefficient is used ($h_c = 10^{10}$), the surface temperature will follow the air temperature exactly (Polivka and Wilson 1976).

The surface of the dam releases electromagnetic radiation, known as thermal radiation, as a result of temperature difference between the surface of the dam and the air. This radiation is measured by the Stefan-Boltzmann law:

[3.6] $$q_r = -e\, C_s\, (T_a^4 - T^4)$$

in which e is the emissivity of the surface; C_s is the Stefan-Boltzmann constant given as 5.669 x 10^{-8} W/m². Note that within the range of temperature differences between the air and the concrete surface, heat loss by radiation is not expected to be significant. It is then possible to rewrite equation [3.6] in a quasi-linear form (Mirambell and Aguado 1989; Elbadry and Ghali 1983):

[3.7] $$q_r = -h_r\, (T_a - T)$$

where h_r is defined as

[3.8] $$h_r = e\, C_s\, (T_a^2 + T^2)(T_a + T).$$

Therefore, the effects of radiation may be considered by adding h_r to h_c to obtain a new convection coefficient. For example, Dilger et al. (1983) assumed a value of 4 W/ (m^2 °K) for h_r in the analysis of a composite box girder bridge in northern British Columbia. In this study a preliminary analysis was conducted, excluding radiation, and the average difference between the surface and air temperature was then used to obtain an average value of h_r.

3.2.2 Concrete-Water Interface

Whether there is water flow or not along the dam-water interface, there will be a small error by assuming that the concrete temperature is equal to the water temperature. This is because for a thick dam the heat transfer and the related dam-water interface thermal gradient will be small. Therefore, it is assumed that the concrete temperature variations are identical to the water temperature fluctuations at the dam-water interface. Thus, no convection and radiation is assumed to occur at this boundary. The concrete temperature in contact with the water is therefore prescribed in time in the mathematical model. This is similar to specifying displacement boundary conditions in structural analysis.

3.2.3 Concrete-Foundation Interface

The dam-foundation interface represents a discontinuity extending across the entire cross-section. Moreover, a finite element model of a dam fixed at the dam-foundation interface will develop an unrealistically large amount of restraint at the base of the dam. A foundation model has therefore been developed for this study. It is assumed that only heat transfer by conduction occurs at the concrete-foundation interface. If there is water flowing at the dam-

foundation interface, the heat transfer mechanism will be affected. To avoid the finite element representation of the foundation, an adiabatic condition has sometimes been used at the dam-foundation interface (Veltrop et al.1990) It should be noted that near the heel, the concrete temperature will be very close to the water temperature, while near the toe the concrete temperature will be influenced by the air temperature.

3.3 Initial Conditions

The cyclical boundary temperature variations will ultimately control the temperature in the dam after the hydration heat developed during construction has dissipated. Convergence is obtained when a repetitive mean annual concrete temperature time history is observed (Paul and Tarbox 1991). To compute the mean concrete temperature, the average temperature of each element is calculated from the nodal temperatures. The resulting temperature is then multiplied by the volume of the element. A summation of these weighted temperatures is carried out for all the elements of the dam (or for a selective group of elements). The result is then divided by the sum of the concrete element volumes to obtain the mean concrete temperature. To obtain a rapid convergence of the solution, the initial temperature distribution at time zero should be defined as near to the final reference temperature condition as possible. To determine an initial temperature distribution, a steady-state heat transfer analysis is carried out by applying the mean annual air, water, and foundation temperatures directly at the boundaries of the system. The effect of solar radiation is taken into account by increasing the mean annual temperature of the concrete-air interface above the mean annual air temperature. This increase is based on solar radiation data available from Tarbox (1977) for exposed surfaces at varying slopes, orientations, and latitudes.

CHAPTER 4

Finite Element Model of the Dam-Foundation-Reservoir System

4.1 Geometric Properties

Figure 4.1 shows the dam-foundation-reservoir system analyzed. The typical cross-section of the dam has been adapted from Mlakar (1987). The dam is 90m high, which corresponds approximately to the tallest gravity dams located in Quebec (91m Manic 2, 84m Outarde 3). In this study the same mesh is used for the heat transfer and static stress analysis. The finite element mesh, consisting of four nodes isoparametric elements, has been refined at the top of the dam and near the dam-foundation interface. These are critical locations where seismic induced cracking is likely to occur (Bhattacharjee and Léger 1992). The dam is constituted of jointed monoliths, therefore the system is assumed to be in a state of plane stress for the structural analysis. The dam has been divided into three sections over the height (top, middle, bottom) to compute the mean temperature time histories and to establish critical temperature states. These temperature states will subsequently be used in combination with static loads. The computer program SAP90 (1990, 1989) has been used to carry out the computations.

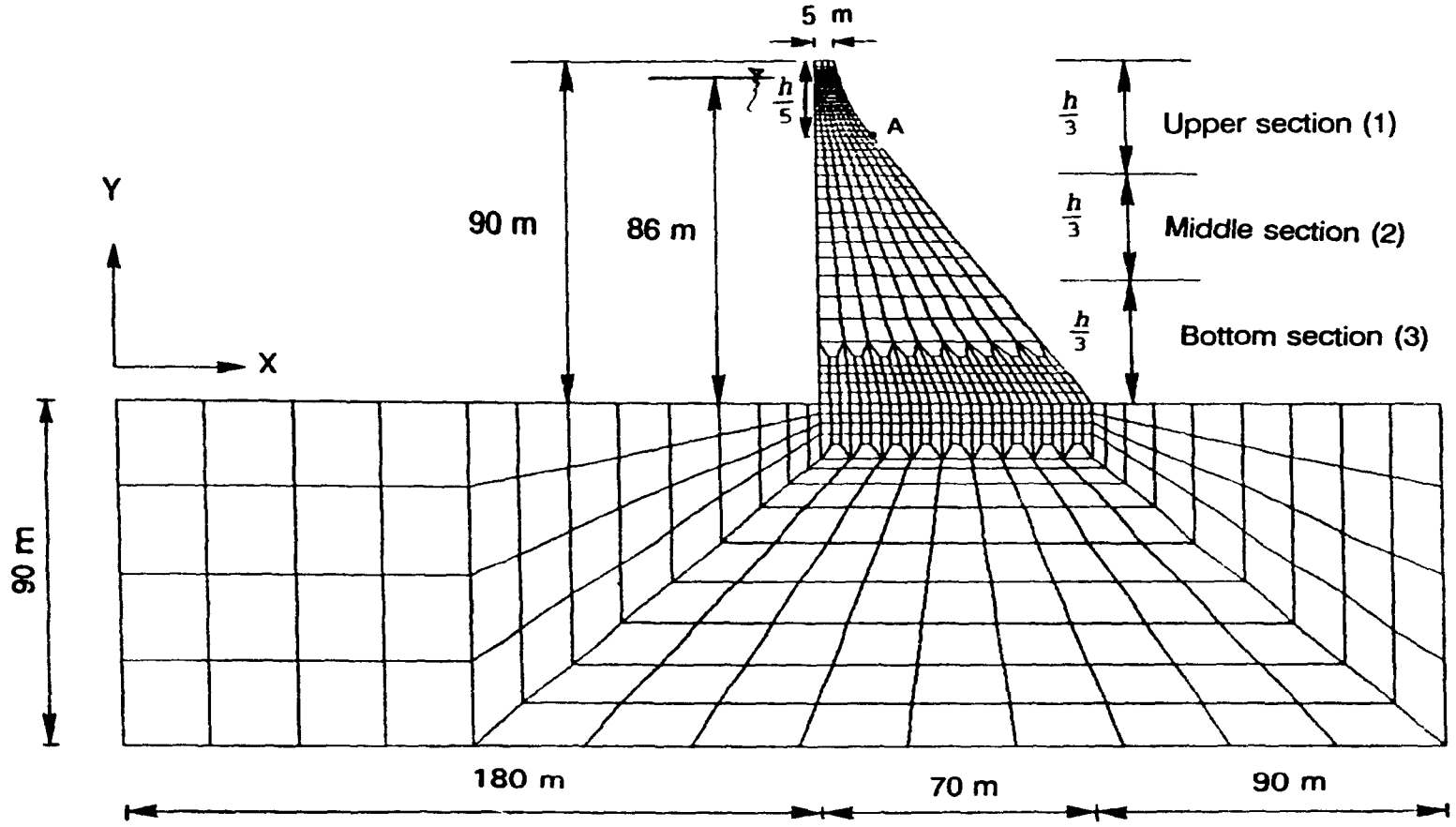

Figure 4.1 Dam-foundation-reservoir system analyzed.

4.2 Material Properties

A range of thermal and elastic properties of mass concrete and rock are listed in Table 4.1 (Jofriet et al. 1990; Gallico and Cavalli 1985; Dilger et al. 1983; ASHRAE 1982; ACI 1981; USBR 1977; Freedman 1974). The selected thermal properties were assumed to be independent of temperature. The absorptivity and emissivity values for concrete are dependent on the surface condition. If the surface is clean, the absorptivity factor is between 0.5 and 0.65 while the emissivity factor is between 0.65 to 0.9. If a film of ice or a layer of fine fresh snow or frost is present, these values are affected. Dilger et al. (1983), in an analysis of thermal effects on composite box girder bridges, have mentioned values of 0.96 and 0.31 for emissivity and absorptivity when a film of ice is present, and 0.91 and 0.13 when a layer of snow or frost is present.

The convection coefficient is a function of the wind speed and of the material properties. Values for the convection coefficient may be obtained from the ASHRAE Handbook (1985) or by using the following approximate equation for wind blowing over and parallel to a surface (Kreith and Kreider 1981):

[4.1] $$h_c = 3.8\ V + 5.7 (W/m^{2o}K)$$

in which h_c is in W/ (m^{2o}K) and V is the wind speed in m/s.

Table 4.1 Mechanical and thermal properties of system analyzed.

	Concrete	Rock
Thermal Properties:		
Specific Heat, c, J/(kg°K)	870-1080 (912)*	840
Thermal Conductivity, k, W/(m°K)	1.47-4.38 (2.62)	2.42-3.46 (2.42)
Coefficient of Thermal Expansion, α, 10^{-6}/°K	7.2-11.2 (8.9)	3.6-12.8 (8.9)
Convection Coefficient, h_c, W/(m^2°K)	23.2**	-
Linearized Radiation Coefficient, h_r, W/(m^2°K)	4.2	-
Solar Absorptivity, a	0.5-0.65 (0.5)	-
Emissivity, e	0.65-0.9 (.88)	-
Mechanical Properties:		
Modulus of Elasticity, E, MPa	27960	27960
Density, ρ, kg/m^3	2400	2400
Poisson's ratio, υ	0.2	0.33

* Values used in numerical model
** For wind speed of 4.6 m/sec.

4.3 Critical Thermal States and Load Combinations

The critical temperature states for the structural safety of the dam can be broadly classified as: (i) the state that produces the highest upstream principal tensile stresses, (ii) the state that produces the highest downstream principal tensile stresses, and (iii) the state that produce the largest principal compressive stress (Paul and Tarbox 1991). To account for the uncertainties and joint occurrence of different load conditions, several load combinations dealing with "usual", "unusual" and "extreme" loadings, and related performance criteria, are generally defined (USBR 1987). Usual temperatures are defined from "mean design conditions". Unusual temperature conditions are generally defined from an expected value, obtained from the mean

condition, plus some constant times the standard deviation (Dungar 1991). In this study, numerical results have been obtained for the usual temperature conditions.

4.4 Evaluation of Thermal Stresses

The magnitude of the thermal stresses depends on the temperature field, the mechanical properties of the concrete, and the nature of the restraints. Thermal stresses are generally not proportional to the temperature field within the structure as defined by thermal gradients, or minimum temperature drop. Under long term action of stress, creep gives rise to an increase in concrete strain relieving some of the induced temperature stresses. The concrete creep mechanism depends on several factors such as the age of the structure at loading, duration and time variation of loading, temperature, and humidity. A rigorous stress-creep-temperature interaction study requires a coupled step-by-step stress-creep-temperature interaction analysis which is beyond the scope of the present study. To obtain reasonable results, consistent with the current state-of-practice, the temperature stresses, σ_T, induced over a relatively long period (t-t′) can be estimated from:

[4.2]
$$\{\sigma_T\} = [D]\{(1-\psi)(\epsilon-\epsilon_i)\}$$

with

[4.3]
$$\psi = \frac{\chi\phi(t,t')}{1+\chi\phi(t,t')}$$

where [D] is the plane stress material stiffness matrix; $(\epsilon-\epsilon_i)$ is the elastic strain resulting from restraint effects on the unrestrained (stress-free) temperature strain, ϵ_i, without taking creep effects into consideration; ψ $(0 \le \psi \le 1)$ is the relaxation coefficient defined in terms of the aging

coefficient, χ, that accounts for creep under gradually applied stress; $\Phi(t,t')$ is the usual creep coefficient. For example, seasonally induced temperature tensile stresses are varying from zero to their maximum value over a period of approximately 3 months. Using creep related data available from MacGregor et al. (1985) and Ghali and Favre (1986) the relaxation coefficient is estimated as $\psi=0.35$, that is, the long term temperature stress will be approximately 65% of the results obtained by a short term elastic analysis. These results are consistent with the current state of practice which recommends a reduction of 20% to 40% of the instantaneous modulus of elasticity for thermal stress computation (Hayward el al 1991; USBR 1977).

The theoretical stress-free reference temperature state is likely to be affected by mass cooling, creep effects, and seasonal temperature cycles. For old dams, Paul and Tarbox (1991) suggest that a reasonable assumption would be to utilize the mean annual concrete temperature of a reasonably thick dam as the reference temperature to establish thermal gradients and compute related stresses. Concrete cracking is assumed to occur when the tensile stress from the combined action of all loading conditions are exceeding the tensile strength. The tensile strength of concrete used in dam construction ranges from 1.5 MPa to 3.5 MPa with a typical value in the order of 2 MPa. The temperature induced stresses in an initially cracked region will generally be smaller than in an uncracked region. Seasonal temperature and stress distributions in initially damaged concrete dams requires further study.

CHAPTER 5

Environmental Parameters

5.1 Introduction

Seasonal variations of air, reservoir, and foundation temperatures as well as incident solar radiation are established for the northern region of Quebec, near the Baie-Comeau region, were several dams are located (Fig. 1.2 Manicouagan-Outarde region).

5.2 Air Temperatures

Based on available temperature records, a typical design year of 365 days was obtained. The daily temperature records were obtained from the Quebec Ministry of Environment for a weather station located at Manic 2. The records cover a 22 year period, from 1967 to 1989. The daily design temperatures were obtained by averaging the recorded temperatures. The average daily and the monthly design air temperatures are shown in Fig. 5.1a. The minimum average daily air temperature, -19.4 °C, occurs in January, while the maximum average daily air temperature, 19.8 °C, occurs in July.

If no daily temperature record is available for a region, the air temperature may be

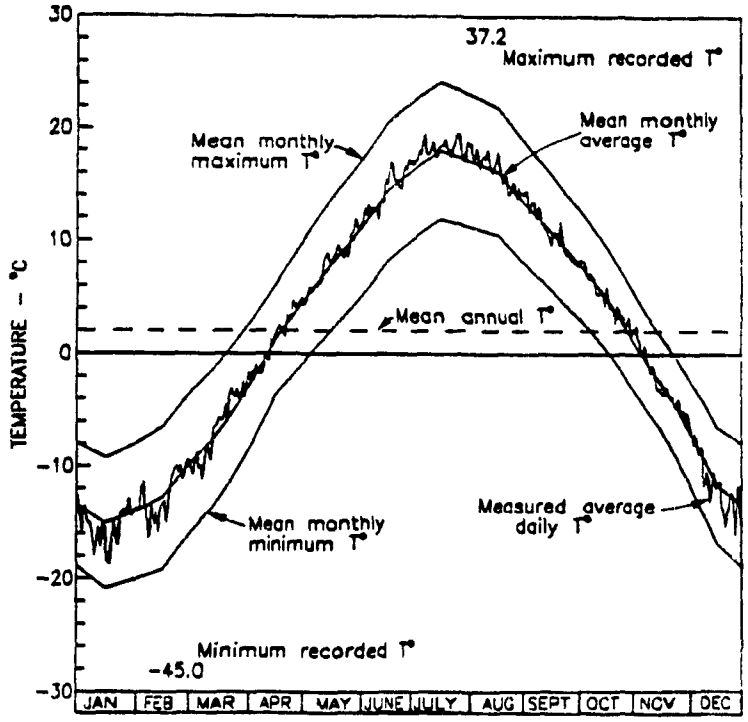

(a)

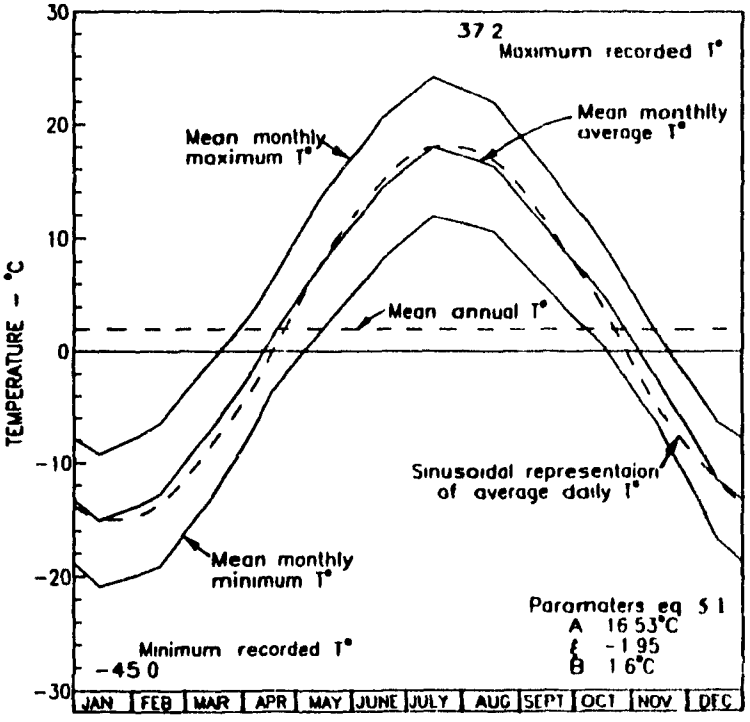

(b)

Figure 5.1 Average air temperatures: (a) daily and monthly average; (b)sinusoidal representation of daily average temperature.

approximated by the following sinusoidal function (Fig. 5.1b; adapted from Tarbox 1977):

[5.1] $$T_a(t) = A \sin\frac{2\pi(t-\xi)}{P} + B$$

where

[5.2] $$A = 0.5 \times(\mid T_{max} - T_{mean} \mid + \mid T_{min} - T_{mean} \mid)$$

in which A is the amplitude of the sine wave, in °C; t is the time, in days; ξ is the lag factor, in radians; P is the period of the sine function, 365 days; B is a constant, in °C; T_{max} is the maximum average monthly temperature, in °C; T_{min} is the minimum average monthly temperature, in °C; T_{mean} is the yearly mean average temperature, in °C. Available data may be used to represent other locations if it is adjusted for latitude and elevation. The temperature should be decreased by 0.55 °C for an increase of 1.4° in latitude, and by 0.55 °C for an increase of 77m in elevation (Tarbox 1977; USBR 1977).

The average wind speed at Baie-Comeau, 4.6 m/s west, is assumed to represent the area of interest (Environment Canada, atmospheric environment service 1985).

5.3 Solar Radiation

An important source of energy to reach the surface of the dam not covered by water is solar radiation. The total solar radiation that reaches a tilted surface is made up of three components; (i) beam radiation, (ii) sky diffuse radiation, and (iii) ground diffuse radiation (fig. 5.2). Beam radiation reaches the face of the dam directly from the sun. Sky diffuse radiation is solar radiation that reaches the dam surface after its direction has been changed by scattering

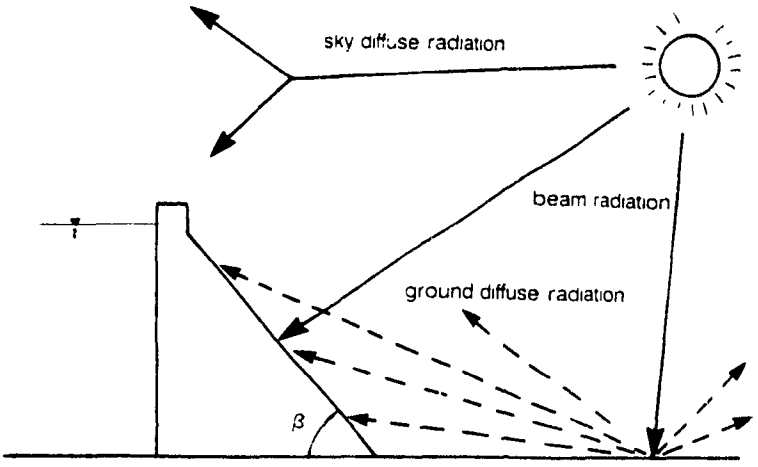

Figure 5.2 Beam radiation, sky diffuse radiation, and ground diffuse radiation.

by the atmosphere. Finally, ground diffuse radiation is solar radiation that is reflected by the ground. The percentage of total solar radiation which is reflected by the ground is a function of the ground cover. Suggested values are 20% when there is no snow cover and 70% when there is snow cover (Duffie and Beckman 1980). The amount of solar radiation reaching the concrete surface follows a cyclical seasonal variation. This variation is a function of; (i) latitude of the site, (ii) orientation of the exposed face, (iii) slope of the exposed face, (iv) topography of the surrounding terrain that may block out certain hours of sunshine (terrain factor, Tarbox 1977; USBR 1977), and (v) time of the day, and the day of the year.

Solar radiation data for the Baie-Comeau region is available from McKay and Morris (1985). Using linear interpolation, the amount of solar radiation reaching the downstream face of the dam was obtained. The solar radiation data is given for an average day of the month. It is assumed that this day occurs at mid month and that a linear variation exists between months. The solar radiation data is given for a surface resting on a flat terrain. To take into account the

topography of the surrounding terrain, the data was modified by the terrain factor. To obtain the terrain factor, the slopes of the terrain on the side of the dam along an east west profile are extended; the angle between these two lines, divided by 180°, is the terrain factor (Tarbox 1977). A terrain factor of 0.75 was calculated for this study by using a typical profile found in the area of interest. The amount of solar radiation reaching a surface facing south east at an inclination of 52° is shown in Fig. 5.3.

Data for solar radiation reaching an inclined surface at a particular location and orientation is often not readily available, while data for solar radiation reaching a horizontal surface is more easily obtainable (McKay and Morris 1985). By knowing the beam and diffuse radiation reaching a horizontal surface it is possible to estimate the radiation reaching an inclined surface through the use of transformation equations (Duffie and Beckman 1980). The equations consists of three parts. The first part calculate the beam radiation reaching the tilted surface, the second the sky diffuse radiation, and the third part calculate the ground diffuse radiation reaching the surface:

[5.3] $$I_T = I_b R_b + I_d\left(\frac{1+\cos\beta}{2}\right) + (I_b+I_d)\rho\left(\frac{1-\cos\beta}{2}\right)$$

in which I_T is the total radiation on a tilted surface, in W/m^2 ; i_b is the beam radiation on a horizontal surface, in W/m^2; R_b is the geometric factor; I_d is the diffuse radiation on a horizontal surface, in W/m^2; β is the tilt of surface measured from the horizontal, in degrees; ρ is the diffuse ground reflectance (0.2 when no snow cover is present and 0.7 when snow is present).

The geometric factor, R_b, is the ratio of the beam radiation on a tilted surface to that on a horizontal surface . The geometric factor is given by:

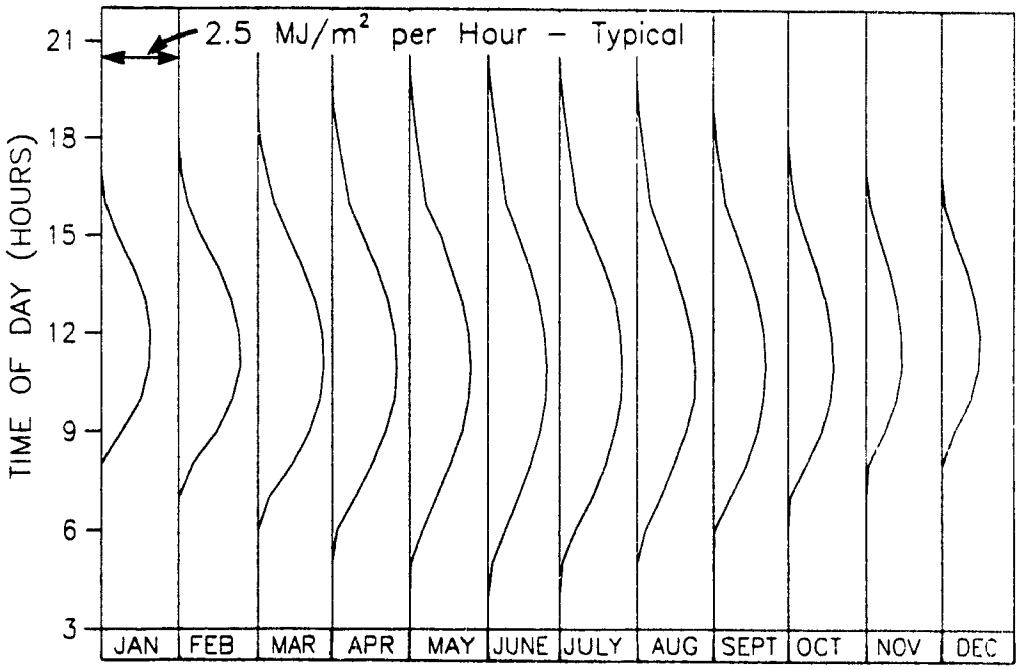

(a)

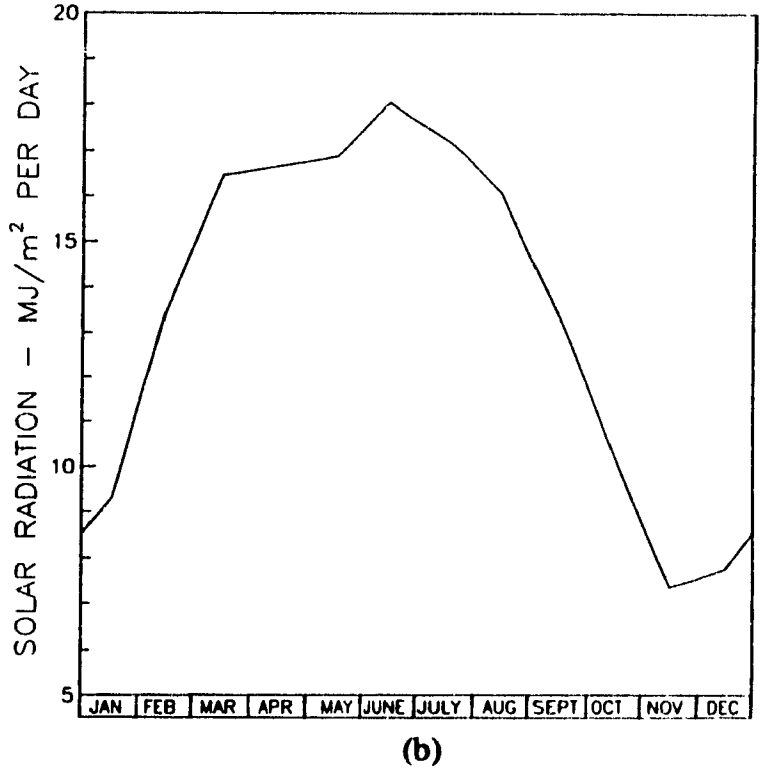

(b)

Figure 5.3 Variation of solar radiation for a surface facing south east with a 52° inclination and for an absorptivity of 1.0 and a terrain factor of 1.0: (a) typical hourly variation; (b) daily variation.

[5.4] $$R_b = \frac{\cos\theta}{\cos\theta_z}$$

in which Θ is the angle between the beam radiation on a surface and the normal to that surface (fig. 5.4a); Θ_z is the angle between the beam radiation on a horizontal surface and the normal to that surface (fig. 5.4b).

Theta, Θ, is given by:

[5.5] $$\cos\theta = \sin\delta\sin\phi\cos\beta - \sin\delta\cos\phi\sin\beta\cos\gamma + \cos\delta\cos\phi\cos\beta\cos\omega \ldots$$
$$\ldots + \cos\delta\sin\phi\sin\beta\cos\gamma\cos\omega + \cos\delta\sin\beta\sin\gamma\sin\omega$$

in which Φ is the latitude, north of the equator is positive, $-90^\circ \leq \Phi \leq 90$; δ is the declination, the angular position of the sun at solar noon with respect to the plane of the equator, north positive, $-23.45^\circ \leq \delta \leq 23.45^\circ$; γ is the surface azimuth angle, the deviation of the projection on a horizontal plane of the normal to the surface from the local meridian, with zero due south, east negative, west positive, $-180^\circ \leq \gamma \leq 180^\circ$ (fig. 5.4c); ω is the hour angle, the angular displacement of the sun east or west of the local meridian due to rotation of the earth on its axis at 15° per hour, morning negative, afternoon positive.

For a horizontal surface β is zero, and the angle of incidence is the zenith angle of the sun, θ_z. Equation 5.5 reduces to

[5.6] $$\cos\theta_z = \cos\delta\cos\phi\cos\omega + \sin\delta\sin\phi$$

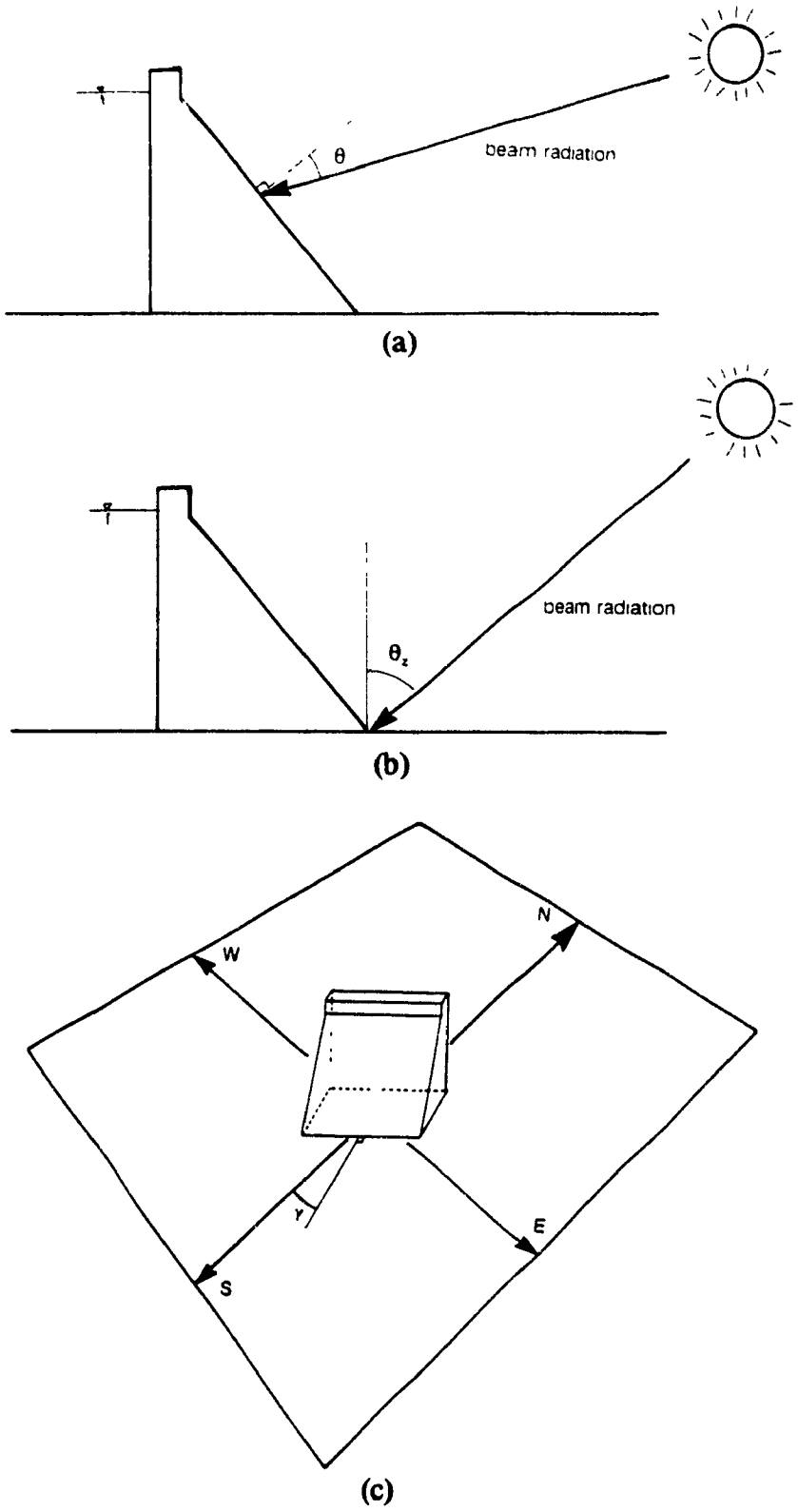

Figure 5.4 Angles in solar radiation equations; (a) Θ; (b) Θ_z; (c) γ.

Declination may be found by:

$$[5.7] \qquad \delta = 23.45 \sin\left(360\frac{284+n}{365}\right)$$

where n is the day of the year. Table 5.1 shows the day of the month that should be used to obtain an average monthly value.

Using the data available from McKay and Morris (1985) for hourly radiation reaching a horizontal surface, the hourly solar radiation reaching the face of the dam was calculated (fig 5.3b). Equations [5.3]-[5.7] were also used to calculate the solar radiation reaching the dam at the middle of the month and these were compared to the values obtained from McKay and Morris. As may be seen from table 5.2, the average difference is 11%. The snow cover was assumed to be present from November to March. For April, an average for ρ was used.

5.4 Reservoir Temperatures

Reservoir temperature varies with depth and follows a cyclical seasonal variation. The temperature can vary significantly from one site to another due to reservoir geometry, environmental conditions acting at the surface (such as wind, temperature, and ice cover), the inflow of water, and the operating conditions. There is no simple rule to define a reservoir temperature profile. Closed form expressions to obtain the reservoir temperature profile, and its variation with time, have been suggested by Bofang and Zhanmei (1990) for arch dams located in the People's Republic of China. However, general use of these expressions is questionable, especially if an ice cover is present for a significant part of the year. Additional information available from the literature has been used in this study to develop mathematical models to establish temperature profiles in the reservoir (Paul and Tarbox 1991; Veltrop et al.

Table 5.1 Recommended average day for each month and values of n by months (Duffie and Beckman 1980)

Month	Date	n, Day of the Year	δ, Declination
January	17	17	-20.9
February	16	47	-13.0
March	16	75	-2.4
April	15	105	9.4
May	15	135	18.8
June	11	162	23.1
July	17	198	21.2
August	16	228	13.5
September	15	258	2.2
October	15	288	-9.6
November	14	318	-18.9
December	10	344	-23.0

Table 5.2 Solar radiation at mid month based on equations by Duffie and Beckman (1980).

	Solar Radiation at Mid Month - MJ/m^2 per day		
Month	Equations	Measured	Percent Difference
January	7.8	9.3	20
February	11.6	13.4	16
March	15.1	16.5	9
April	15.7	16.7	6
May	15.9	16.9	6
June	17.2	18.0	5
July	16.3	17.1	5
August	15.0	16.1	7
September	12.2	13.3	9
October	9.2	10.3	12
November	6.6	7.4	11
December	6.4	7.8	22

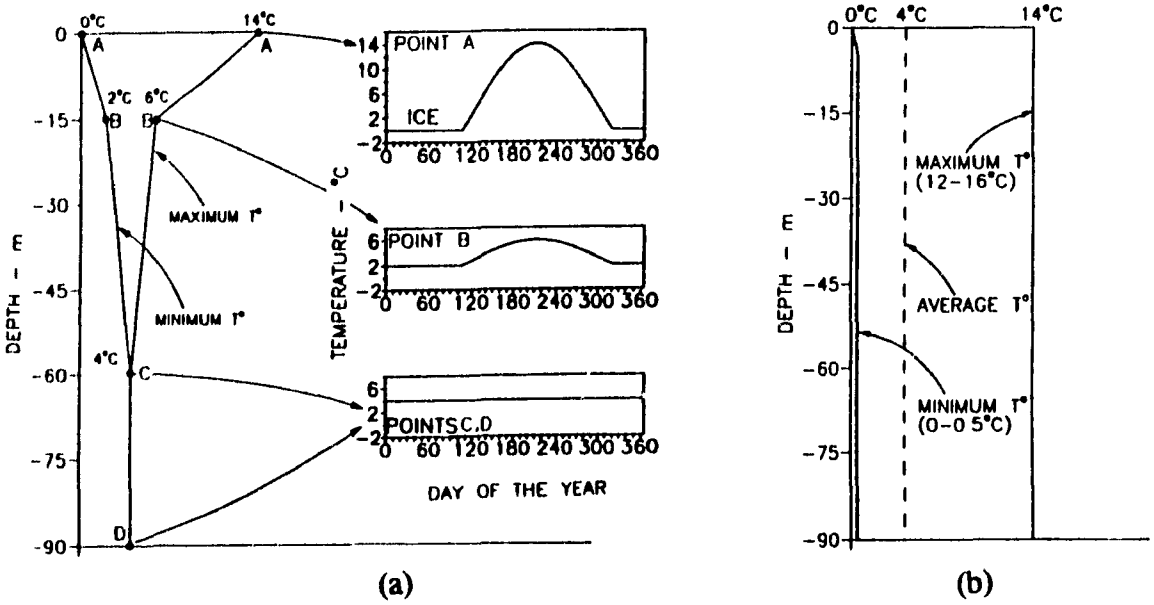

Figure 5.5 Reservoir temperature profiles: (a) deep reservoirs with small water intake with respect to their volumes; (b) shallower reservoirs with important inflow of water with respect to their volumes.

1990; Marcotte et al. 1977; Tarbox 1977). Two types of reservoirs with different temperature profiles are generally recognized as is shown in Fig 5.5. The first type is formed by a deep reservoir with small water intake with respect to its volume (Fig. 5.5a). The second type of reservoir has an important inflow of water with respect to its volume and is usually shallower (Fig. 5.5b).

The temperature profile used for the reservoir in the preliminary study is shown in Fig. 5.5a. The maximum surface temperature is assumed to occur at the end of July, beginning of August. The ice period is assumed to be from about November 15 to April 15. During this period it is assumed that the ice insulates the reservoir, therefore no temperature fluctuation is occurring. During the ice free season, surface conditions are assumed to cause the water temperature to fluctuate in time. Throughout the reservoir depth, this time fluctuation is assumed

to follow a sine curve representation. Since 3 points on the sine curve are known, equation [5.1] is used to obtain the temperature profile.

5.5 Foundation Temperatures

The depth of penetration of annual temperature oscillations in the foundation is assumed to be 10m (ASHRAE 1982). Below this depth the soil temperature increases due to the geothermal gradient as shown in Fig. 5.6 (Hammer et al. 1985). The geothermal gradient is assumed to be 3 °C per 100 m (Gupta 1980) . Temperature measurements for the first 3m of soil are available for Normadin (49 °N latitude, 72 °W longitude), which is close to the area of interest (Environment Canada, atmospheric environment service 1984). Based on interpolation of the available data, the soil temperature at 10m is assumed to be 5 °C . The temperature at the base of the foundation (90 m) is therefore 7.7 °C. Note that snow insulates the soil against air temperature during the winter months. The soil temperature at the bottom of the reservoir is assumed to be at the same temperature as the water at this location; 4 °C for the type I reservoir used (fig. 5.5a). The temperature profile used for the exposed foundation is also used here, with the exception that the top layer is at 4 °C.

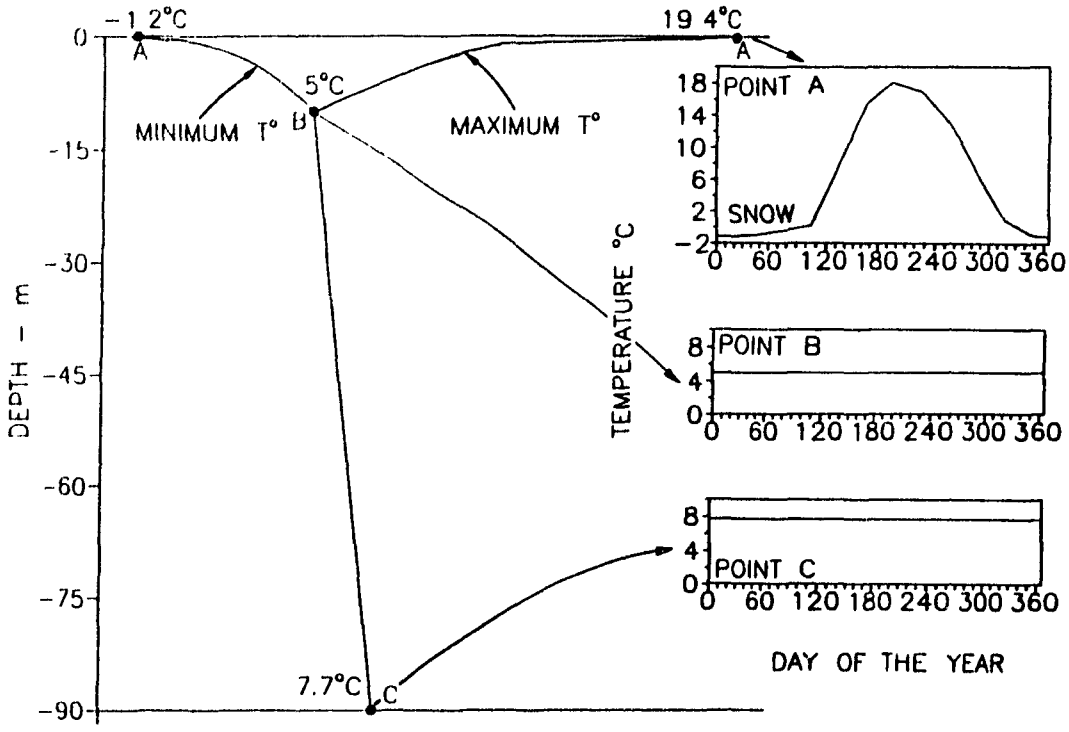

Figure 5.6 Foundation temperature profile.

CHAPTER 6

Seasonal Variations of Temperature and Stress Distributions

6.1 Convergence of Heat Transfer Analysis

Figure 6.1 shows the time history of the average temperatures for the dam and sections 1, 2, and 3 (fig. 4.1), using a time step of one day. A smaller time step of half a day was found not to affect the results. Convergence, which is obtained for the second year of analysis, is defined when the average concrete temperature evaluated on January 1st did not vary by more than 1% for sections 1, 2, or 3. If, as a convergence criteria, the temperature of a node located at the centre of each section is considered, convergence is achieved on the third year. It was decided to use the 365 temperature distributions obtained for the third year to represent the typical variations of "seasonal temperature" distributions.

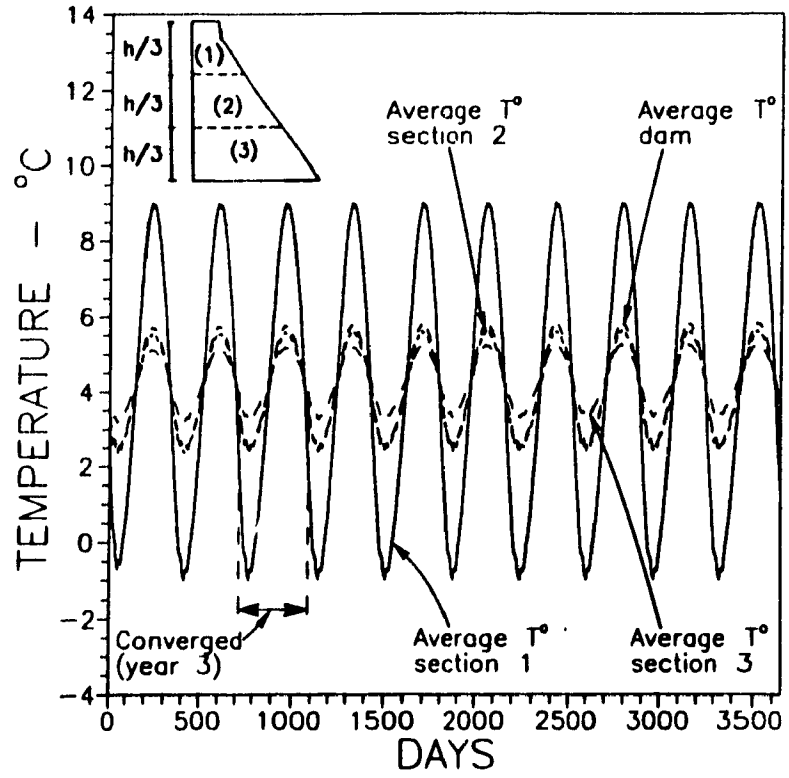

Figure 6.1 Convergence of mathematical solution.

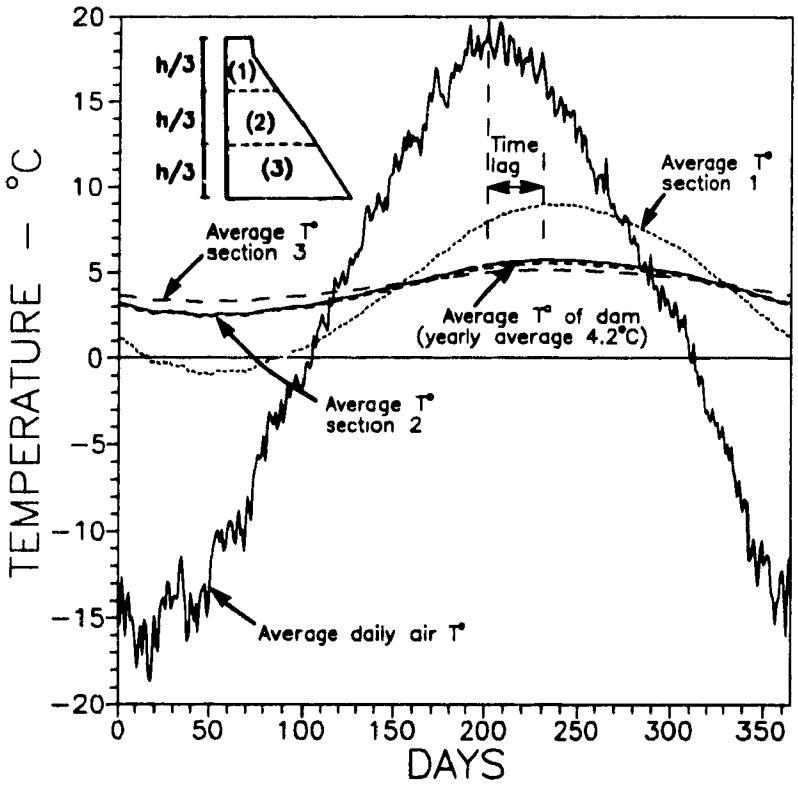

Figure 6.2 Average thermal response of the dam.

6.2 Transient Thermal and Stress Response

After convergence of the heat transfer analysis, 365 daily temperature distributions, that are assumed to be representative of a typical yearly response, are obtained. Figure 6.2 shows the average thermal response of the dam due to seasonal variations of air, reservoir, foundation temperatures and solar radiation. The average temperature variations for the top, middle and bottom third sections of the dam are in phase. Due to thermal inertia, a time lag of approximately 30 days is observed between the time at which the minimum (maximum) average temperature of the dam is reached, and the time at which the minimum (maximum) air temperature is occurring. The annual average concrete temperature for the complete dam was computed as 4.2 °C, as compared with an annual average air temperature of 2.1 °C without solar radiation and of 6.4 °C when solar radiation is accounted for. A reference temperature of 4.2 °C will thus be used to evaluate the thermal stresses. A reference temperature of 5 0 °C was obtained for the foundation.

6.3 Yearly Temperature and Stress Distributions Envelopes

To study the temperature and stress distributions in the dam, weekly temperature distributions were used to carry out 52 stress analyses. Figure 6.3 shows the typical temperature stress time histories for node I, located at the dam-air interface, and node II, located 4m within the dam. The stresses variations at I are in phase with the air temperature variations. The stress drop between peaks is 70%, and a lag time of 175 days occurs between peaks. Moreover, location II, within the dam, is in a biaxial stress state, while location I, on the outside surface,

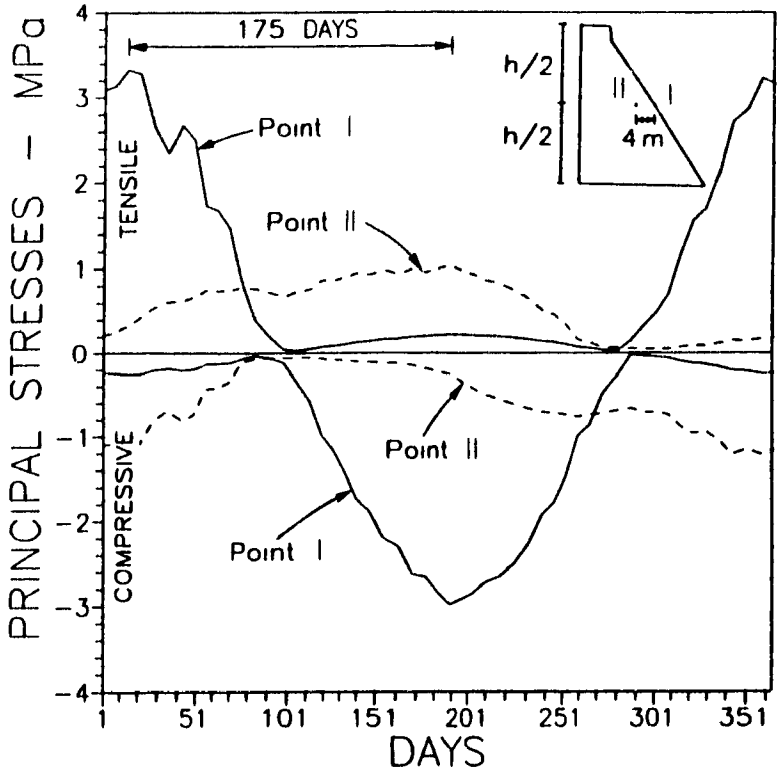

Figure 6.3 Time history of stresses within outer concrete shell.

is in an uniaxial stress state.

Figure 6.4a presents an envelope of minimum temperature distribution based on 365 daily heat transfer analysis results. High thermal gradients are occurring along the downstream face exposed to air over a depth of approximately 5 m. The bulk of the dam never goes below 2°C, while the downstream face may reach approximately -16 °C. Figure 6.4b shows contours of the days at which the minimum temperatures shown in Fig. 6.4a have been reached. The contour lines are parallel, the deeper inside the structure, the longer the time lag to reach the minimum temperature. From Fig. 6.4a the maximum depth of frost penetration for a 90m dam

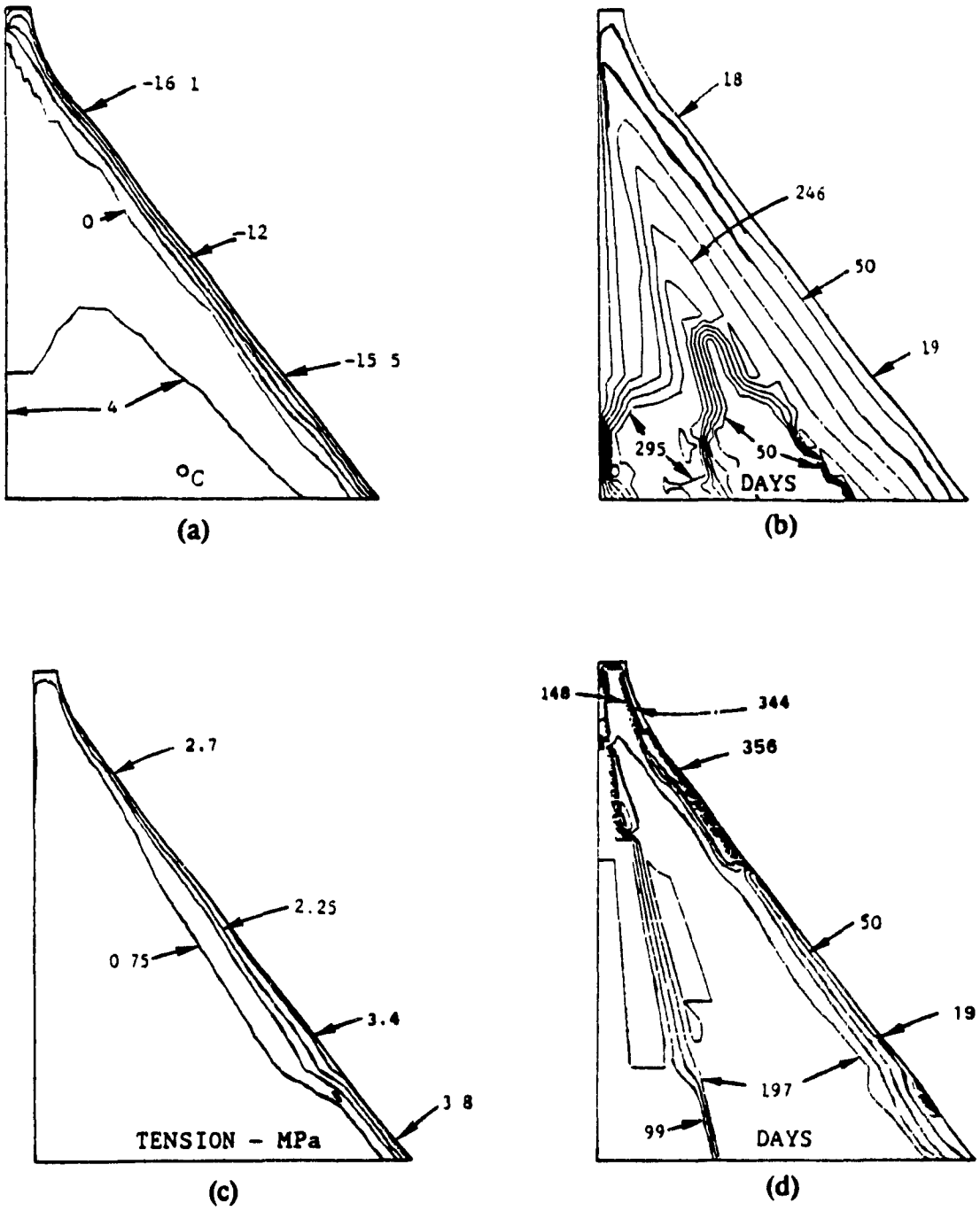

Figure 6.4 Tensile stresses: (a) minimum temperature envelope; (b) day when minimum temperature occurs; (c) tensile stress envelope; (d) day when maximum tensile stresses occur. (Note: temperature contours are at 4 °C intervals, day contours at 49 day intervals, stress contours at 0.75 MPa intervals. Values reported at the surface are maximum values.)

located in the lower St-Lawrence region can be seen as the 0 °C contour line. The depth of frost penetration is almost uniform over the height and is approximately 6m. The maximum frost penetration is occurring in mid March instead of the coldest period of the year due to the thermal inertia of the system in responding to the external air temperature variations.

Figure 6.4c shows an envelope of the highest principal tensile stresses reached within the dam based on 7-day incremental stress analyses using the corresponding temperature distributions computed from the heat transfer analysis. The maximum tensile stress near the downstream face at the toe of the dam is of the order of 3.8 MPa and occurs during the coldest period in December-January. The maximum tensile stress near the downstream face at the top of the dam, in the vicinity of anticipated seismic induced cracking, is of the order of 2.8 MPa and occurs in December-January. Figure 6.4d shows contours of the days at which the maximum tensile principal stress have been reached within the dam. It is obvious that a few critical times must be selected to define temperature distributions that will maximize the stress response in different zones of the dam for subsequent combinations with self-weight, hydrostatic, seismic and other loads.

Figure 6.5 shows the stress results obtained for the maximum temperature distribution. The maximum increase in compressive stresses is of the order of 3.4 MPa and is located near the toe of the dam. Compressive stresses are usually not of a concern, but problems may arise when sections of the dam have different orientations. For example, Fontana dam experienced cracking in the summer due to a longitudinal thrust in the curved section of the dam caused by the southern exposure of the downstream face, a gradual warming of the concrete mass after construction, and temperature sensitive alkali-silicate reactivity (Abraham and Sloan 1978).

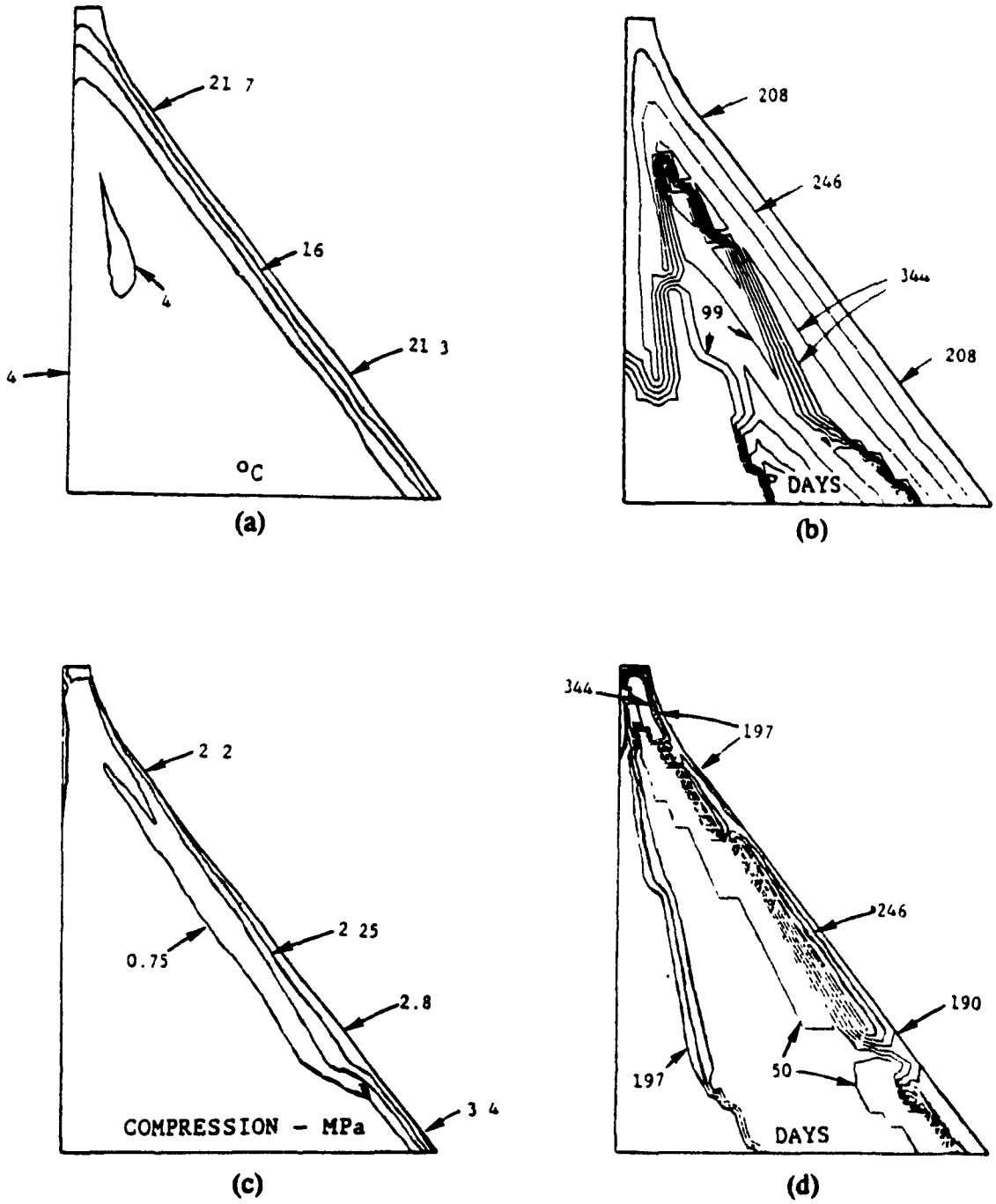

Figure 6.5 Compressive stresses: (a) maximum temperature envelope; (b) day when maximum temperature occurs; (c) compressive stress envelope; (d) day when maximum compressive stresses occur.

6.4 Critical Temperature and Stress Distributions for Structural Safety analysis

To determine the critical tensile thermal stresses and related temperature distributions on the downstream face, a study of the thermal gradients computed at various sections along the dam height from the difference in temperature between the node located at the outside surface, and the first node within the dam has been carried out. The time at which the maximum surface thermal gradient (critical gradient) occurs corresponds to the time of maximum stress. However, this is not true for any other pair of consecutive nodes located within the dam. Figure 6.6 shows the resulting critical temperature and stress distributions for maximum downstream tensile stresses at the top and bottom regions of the dam.

Seasonal temperature variations provide significant tensile stressing mechanism in the vicinity of the downstream face. Therefore, in a safety analysis it would be appropriate to combine the temperature effects with the seismic effects and other relevant loads to evaluate the performance of the dam. Although it is possible that the maximum temperature induced tensile stresses occurs simultaneously with the Maximum Credible Earthquake (MCE), this joint probability of occurrence is small. The return period for this load combination, that should be considered in the safety evaluation, is obviously greater than the return period of the MCE. To obtain a more "probable" thermo-seismic load combination, the temperature distribution inducing average tensile stresses corresponding to half of the maximum value reached at a particular critical location can be considered. Numerical investigations have shown that for the system analyzed, the day of the coldest average concrete temperature for the top section will produce a reasonable value to estimate average tensile stress distribution in the top region as

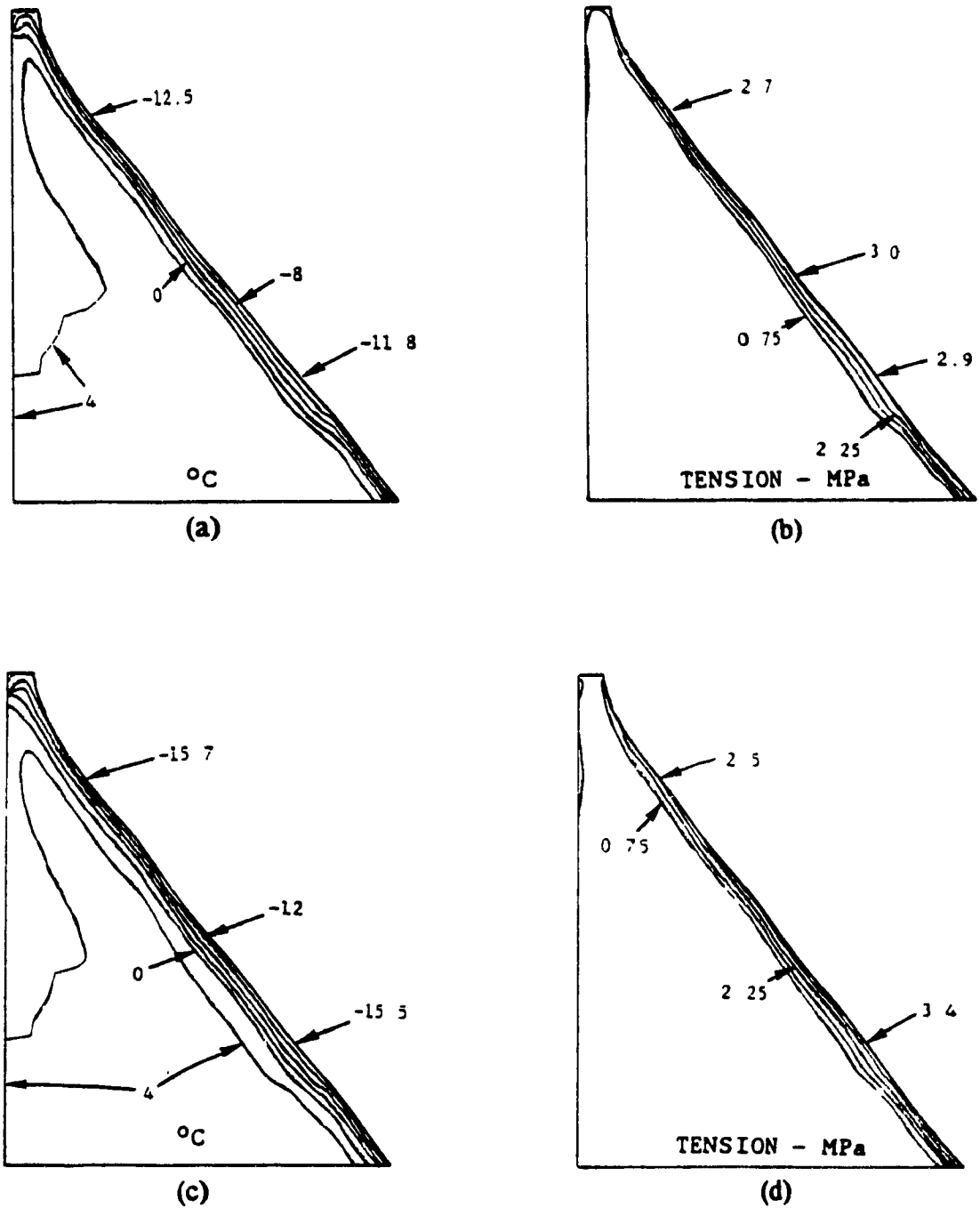

Figure 6.6 Maximum thermal stresses for structural safety evaluation: (a) temperature profile which produces maximum tensile stresses for the top section on the downstream face (day 356); (b) maximum tensile stresses for top section; (c) temperature profile which produces maximum tensile stresses for bottom on downstream face (day 19); (d) maximum tensile stresses for bottom section.

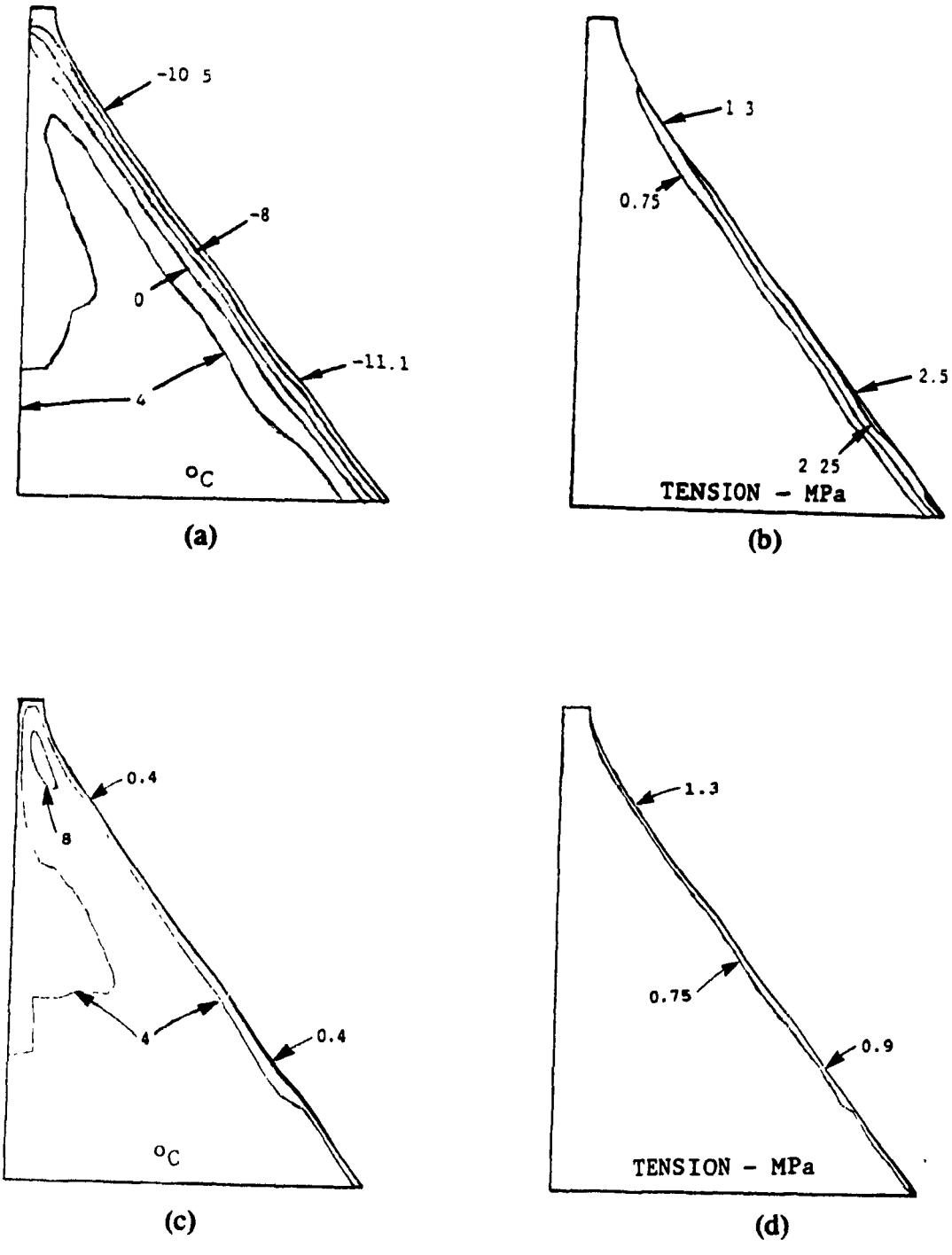

Figure 6.7 Mean stresses for structural safety evaluation: (a) temperature profile when temperature of top section is minimum (day 50); (b) corresponding tensile stresses; (c) temperature profile when surface gradient is half that of the critical temperature gradient (day 317); (d) corresponding tensile stresses.

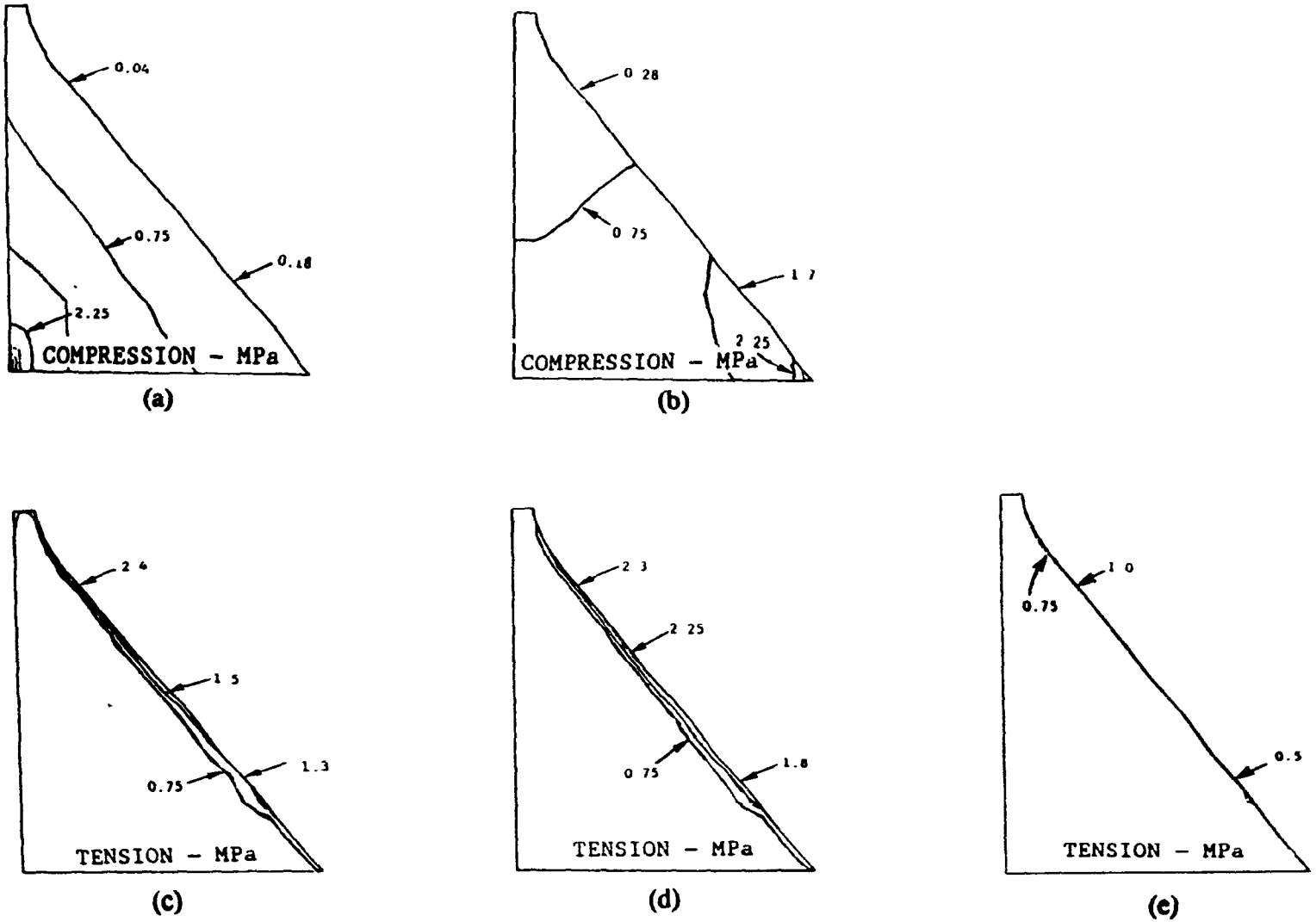

Figure 6.8 Load combinations, stresses due to: (a) self weight; (b) self weight + hydrostatic; (c) self weight + hydrostatic + critical temperature profile for the top section; (d) self weight + hydrostatic + critical temperature profile for the bottom section; (e) self weight + hydrostatic +temperature profile for mean stresses for top section (day 317).

shown in Fig. 6.7. It was also noted that when the thermal gradient between the surface node and a node located at about 1m inside was half that of the critical gradient, mean stresses were obtained. Figure 6.8 shows combined stress distribution due to self-weight, hydrostatic, and temperature loads for critical tensile stress in the top and bottom of the dam, and average tensile response in the top of the dam. Significant thermally induced tensile stresses are observed in the top region of the dam which is most vulnerable for seismic response.

The maximum displacement was obtained on the day when the mean temperature of the top section was minimum.Thermal stresses cause displacements at the crest of the dam varying from +10mm in winter, to -11.2mm in summer. Extreme crest displacement values are reached at times which are close to the days at which the maximum and minimum average concrete temperatures are observed.

CHAPTER 7

Parametric Analyses

7.1 Introduction

The reference air, reservoir, and foundation temperatures, the material properties, and the stress relaxation factor due to creep of the dam-foundation-reservoir system have been previously described. However, there are always uncertainties associated with these parameters. Temperature, and the extent of damage that the structure has received, affects the material properties. Uncertainties in environmental parameters are due to the variability of climatic conditions from year to year, and to the imprecise knowledge of the time history and spatial distribution of temperature and heat fluxes at the boundaries of the dam. Therefore, a parametric analysis is conducted to assess the influence of different modelling assumptions and to identify the most important parameters that affect the structural response of the system. The influence of (i) the geometrical, thermal, and mechanical properties of the dam, (ii) the reservoir, foundation, and air temperature distributions, and (iii) the heat supply from solar radiation, on the stress-strain response of the system, are investigated. Figure 7.1 shows the main response parameters examined in this study. Note that location A is in the zone that is most susceptible to seismic cracking, and that the depth of the 0.75 MPa line is measured on the day when the thermal gradient at location A is critical.

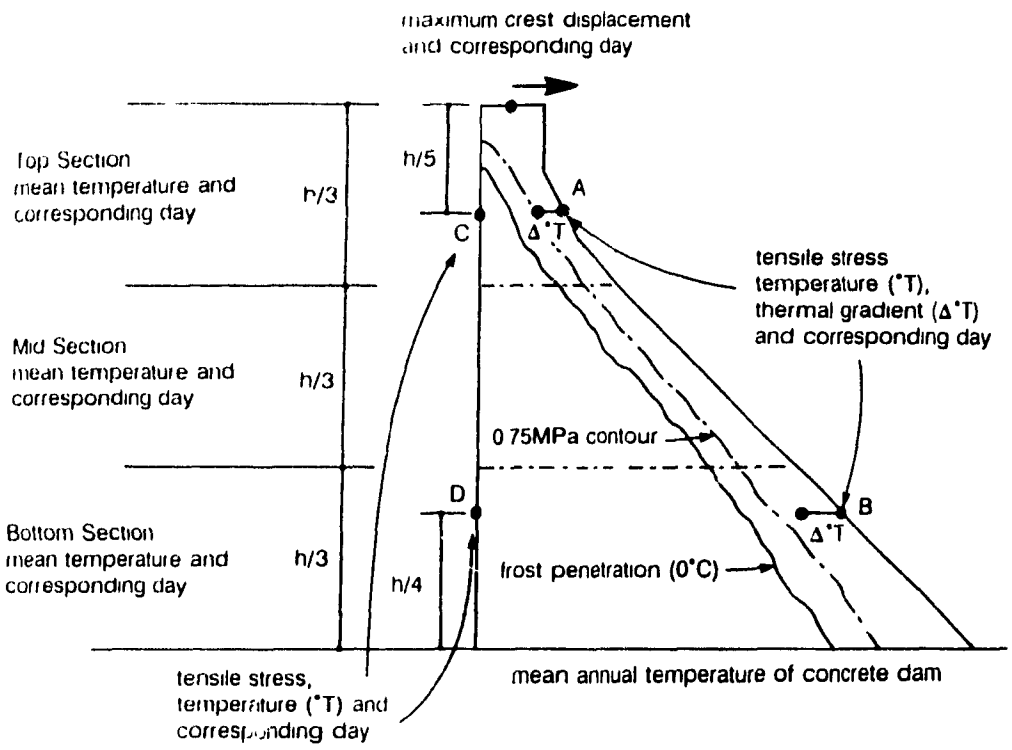

Figure 7.1 Response parameters for parametric analysis.

7.2 Height Effects on Dam Response

The 90m dam-foundation-reservoir model is scaled down to 45m and 22.5m to investigate the effect of height on the thermo-mechanical response. The stress and temperature envelopes, based on 52 weekly runs, are shown in fig. 7.2 for dam heights of 90m, 45m, and 22.5m. Table 7.1 compares the structural response of each dam. As the dam height is reduced, the maximum tensile stress at location A decreases. The maximum tensile stress for the 90m dam (2.7 MPa) is 42% larger than that of the 45m dam (1.9 MPa), and the stress for the 22.5m dam (0.9 MPa) is 53% smaller. The critical day for the maximum stress at location A occurs at about the same time for each height. The stresses at location B for the 90m, 45m, and 22.5m

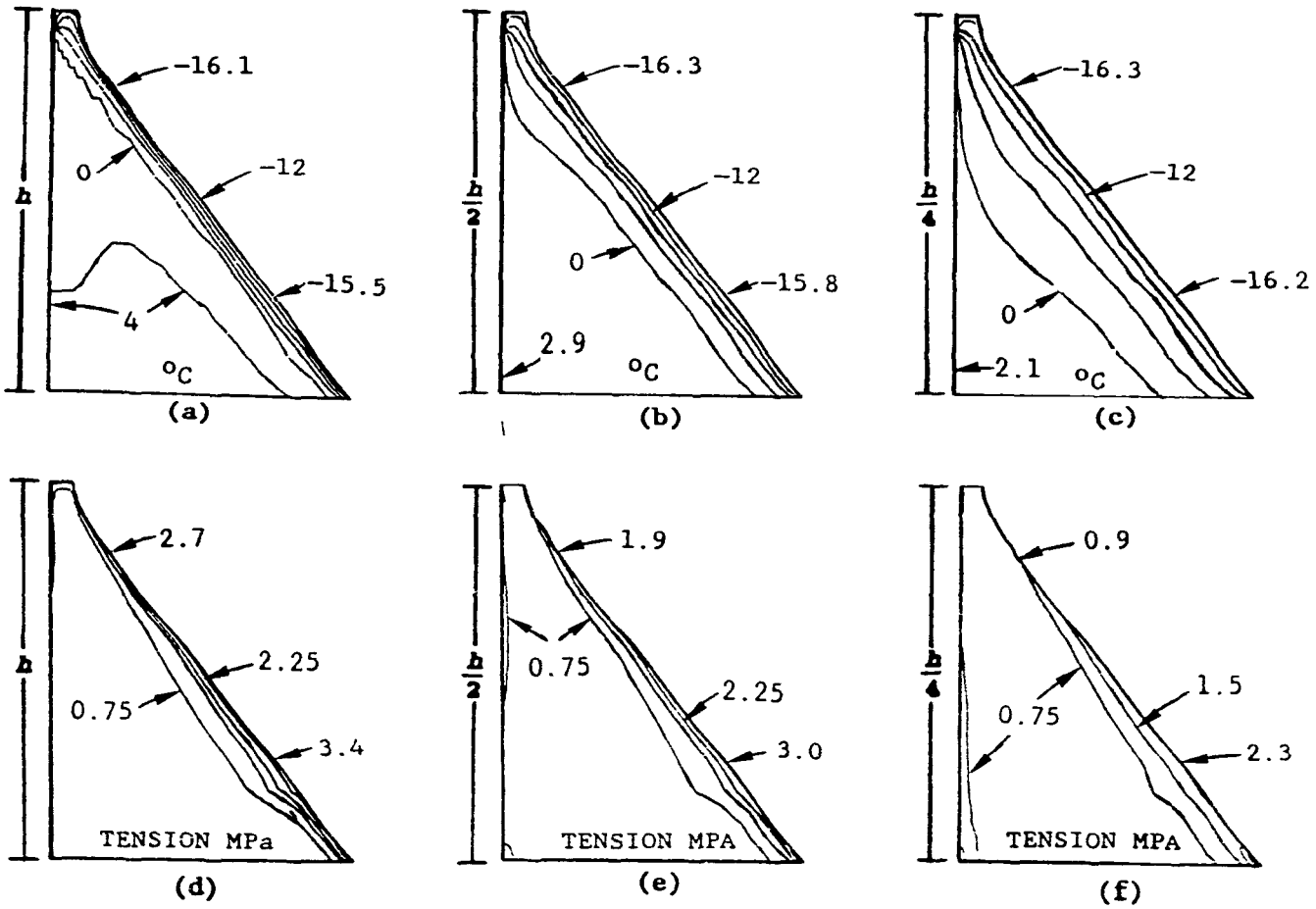

Figure 7.2 Stress and temperature envelope for the 3 dam heights: (a) temperature envelope for 90m; (b) temperature envelope for 45m; (c) temperature envelope for 22.5m; (d) tensile stress envelope for 90m; (e) tensile stress envelope for 45m; (f) tensile stress envelope for 22.5m (note that h=90m).

Table 7.1: Influence of dam height on thermal and structural behaviour.

Response Parameter	Dam Height (m)		
	90	45	22.5
Mean annual °T:			
complete dam (°C)	4.2	4.0	4.1
top section	4.0	4.2	4.1
mid-section	4.0	4.0	4.1
bottom section	4.2	4.1	4.4
Minimum mean °T:			
complete dam (°C,Day)	2.4, 50	0.9, 50	-1.8, 50
top section	-1.0, 50	-4.4, 50	-7.1, 19
mid-section	2.4, 50	0.7, 69	-3.1, 50
bottom section	3.2, 50	2.2, 50	0.0, 69
Minimum surface °T:			
location A (°C,Day)	-16.1, 18	-16.3, 18	-16.3, 18
location B	-15.5, 19	-15.8, 18	-16.2, 18
Critical °T gradient:			
location A (°C,Day)	9.7, 356	5.9, 344	3.1, 343
location B	18.2, 19	13.6, 357	9.0, 356
Max. tensile stress :			
location A (MPa,Day)	2.7, 356	1.9, 344	0.9, 343
location B	3.8, 19	3.0, 357	2.1, 356
Depth of 0.75 MPa[1]:			
location A (m)	2.0	0.9	0.1
location B	4.6	2.2	1.4
Strs.- mean Δ°T at location A:			
location A (MPa,Day)	1.3, 317	1.2, 329	0.6, 315
location B	0.9, 317	1.6, 329	1.2, 315
Frost penetration:			
location A (m)	6.0	6.6	3.5
location B	5.5	5.8	6.5
Max. displacement:			
crest (mm, Day)	10, 5	7, 50	5, 19

1: On day of critical temperature gradient at location A.

dams are 3.8 MPa, 3.0 MPa, and 2.1 MPa, respectively. As the dam height is reduced the mesh spacing is also reduced, therefore, the critical temperature gradients cannot be compared directly.

For the 45m dam, "mean" stress values are not obtained when the mean temperature for the top section is minimum. The stress at location A is 0.6 MPa, which is 69% smaller than the maximum stress of 1.9 MPa. The "mean" stress obtained for the 22.5 dam is 0.4 MPa, which is 56% smaller than the maximum of 0.9 MPa. "Mean" stress values are obtained on the day when the temperature gradient is half that of the critical temperature gradient. When this method is used, the "mean" stress for the 90m dam at location A is 48% of the maximum stress, while for the 45m and 22.5m dams the "mean" stress at location A is about 65% of the maximum stress. This method therefore provides results that are close to half of the critical stress for the 90m dam, and results that represent an upper bound for the 45m and 22.5m dams.

The depth of the 0.75 MPa line decreases as the dam height decreases. At location A, the 0.75 MPa line is at a depth of 2.0m for the 90m dam, 0.9m for the 45m dam, and 0.1m for the 21.5m dam. At location B the 0.75 MPa line is at 4.6m, 2.2m, and 1.4m for the 90m, 45m, and 22.5m dams, respectively.

The mean annual temperatures for the 90m, 45m, and 22.5m dams are 4.2 °C, 4.0 °C, and 4.1 °C, respectively. The difference between each value is less than 5%. As the height decreases, the variation of temperature in the dam increases. The minimum mean temperature for the 90m dam is 2.4 °C, while for the 45m and 22.5m dams the minimum mean temperatures are 0.9 °C and -1.8 °C, respectively. Some reduction in minimum temperature is due to the

reservoir temperature in contact with the dam, where a greater portion of the upstream face is in contact with cold water for dams of limited height. A small change in the stress free reference temperature used for the dam, for example an increase of 1 °C, has a negligible effect on the computed stresses. The foundation reference temperatures for the 90m, 45m, and 22.5m dams are respectively 5.0 °C, 5.2 °C, and 5.0 °C.

The top maximum positive displacements for the 90m, 45m, and 22.5m dams are respectively 10mm, 7mm, and 5mm. The maximum displacements occur when the mean temperature of the top sections are lowest. For the 90m and 45m dams, the minimum mean temperatures for the top section occur on the same day as when the mean temperatures of the complete dams are minimum. If the displacement for the 22.5m dam is calculated on the day when the mean temperature of the complete dam is minimum, a very good approximation is obtained.

The depth of frost penetration for each dam is similar. The average depth of frost penetration at location B is about 6m. The depth of frost penetration at location A for the 45m and 22.5m dams extends through most of the dams' thicknesses, where the thicknesses are 7.3m and 3.7m, respectively. In each case, the reservoir prevents the frost penetration from going through the dam. The maximum depth of frost penetration occurs in mid March for the 90m and 22.5m dams, while for the 45m dam it occurs at the beginning of March.

A significant number of gravity dams located in Quebec have a height close to 45m; therefore, the rest of the parametric analysis is conducted for this height. The presentation of the results will emphasize the magnitude of thermal stresses, and the depth of frost penetration.

7.3 Effects of Concrete Thermal Properties on Dam Response

The convection coefficient, h_c, that regulates the heat exchange between air and concrete is dependent on the wind speed. If no wind is present, the convection coefficient is 5.7 W/(m^2°K). This represents a reduction of 75% from the value when the average wind speed is present (23.2 W/(m^2°K)). To obtain an upper bound the convection coefficient, h_c, is increased by 75% (40.6 W/(m^2°K)). To account for radiation, the linearized radiation coefficient, h_r, is added to the convection coefficient, h_c, (4.2 W/(m^2°K)).

As table 7.2 indicates, the convection coefficient, h_c, has a small effect on the tensile stresses. The major effect is on the depth of frost penetration. When the convection coefficient, h_c, is 5.7 W/(m^2°K) the depth of frost penetration at location B is reduced by 38%. At location A, the depth of frost penetration is not affected by much. This is due to the fact that the section at location A is thinner, therefore the reservoir has a greater influence on the thermal response. When the convection coefficient, h_c, is 40.6 W/(m^2°K) the depth of frost penetration at location B increases by 10%.

The conduction coefficient, k, and specific heat, c, of concrete are a function of the type of aggregate. To investigate the effects of these parameters, upper and lower limits for these parameters are obtained from the literature (ACI 1981). Values of 1.87 W/(m°K) and 3.68 W/(m°K) are selected for the conduction coefficient, k, and values of 870 J/(kg°K) and 945 J/(kg°K) are selected for the specific heat, c. The effects of these parameters are listed in tables 7.2 and 7.3.

Table 7.2. Influence of h_c and k on the thermal and structural behaviour for a 45m dam.

Response Parameter	h_c (W/(m²°K))			k (W/(m°K))		
	5.7	23.4	40.6	1.87	2.62	3.68
Mean annual °T:						
complete dam (°C)	5.8	4.0	3.7	4.1	4.0	4.1
top section	6.2	4.2	3.8	4.2	4.2	4.2
mid-section	5.9	4.0	3.6	4.0	4.0	4.0
bottom section	5.6	4.1	3.8	4.1	4.1	4.1
Minimum mean °T:						
complete dam (°C,Day)	2.6, 50	0.9, 50	0.5, 50	1.3, 50	0.9, 50	0.4, 50
top section	-2.5, 45	-4.4, 50	-4.9, 50	-3.7, 50	-4.4, 50	-5.0, 44
mid-section	2.6, 50	0.7, 69	0.3, 69	1.2, 50	0.7, 69	0.0, 69
bottom section	3.7, 50	2.2, 50	1.9, 50	2.5, 50	2.2, 50	1.9, 50
Critical °T gradient:						
location A (°C,Day)	-12.1, 18	-16.3, 18	-17.3, 18	-16.5, 18	-16.3, 18	-16.2, 18
location B	-11.7, 19	-15.8, 18	-17.0, 18	-15.6, 18	-15.8, 18	-15.6, 18
Maximum surface Δ°T:						
location A (°C,Day)	5.1, 344	5.9, 344	6.1, 347	6.8, 344	5.9, 344	5.0, 344
location B	12.8, 357	13.6, 357	13.9, 356	14.9, 357	13.6, 357	12.3, 357
Max. tensile stress :						
location A (MPa,Day)	1.8, 344	1.9, 344	1.9, 347	2.1, 344	1.9, 344	1.6, 344
location B	2.8, 357	3.0, 357	3.0, 356	3.1, 357	3.0, 357	2.8, 357
Depth of 0.75 MPa[1]:						
location A (m)	0.9	0.9	1.0	1.0	0.9	0.8
location B	2.1	2.2	2.3	2 .2	2.2	2.3
Strs.- mean Δ°T at location A:						
location A (MPa,Day)	1.1, 312	1.2, 329	1.1, 16	1.2, 310	1.2, 329	1.0, 310
location B	0.9, 312	1.6, 329	2.8, 16	0.8, 310	1.6, 329	0.9, 310
Frost penetration:						
location A (m)	6.1	6.6	6.6	6.4	6.6	6.7
location B	3.6	5.8	6.4	4.9	5.8	6.9
Max. displacement:						
crest (mm, Day)	5, 45	7, 50	6, 50	6, 50	7, 50	7, 44

1. On day of critical temperature gradient at location A.

Table 7.3: Influence of c on the thermal and structural behaviour for a 45m dam.

Response Parameter	c (J/(kg°K))		
	870	912	945
Mean annual °T:			
complete dam (°C)	4.1	4.0	4.1
top section	4.2	4.2	4.2
mid-section	4.0	4.0	4.0
bottom section	4.1	4.1	4.1
Minimum mean °T:			
complete dam (°C,Day)	0.8, 50	0.9, 50	1.0, 50
top section	-4.5, 45	-4.4, 50	-4.3, 50
mid-section	0.6, 69	0.7, 69	0.7, 69
bottom section	2.2, 50	2.2, 50	2.2, 50
Critical °T gradient:			
location A (°C,Day)	-16.4, 18	-16.3, 18	-16.3, 18
location B	-15.8, 18	-15.8, 18	-15.7, 19
Maximum surface Δ°T:			
location A (°C,Day)	5.8, 344	5.9, 344	6.0, 344
location B	13.5, 357	13.6, 357	13.8, 357
Max. tensile stress :			
location A (MPa,Day)	1.8, 344	1.9, 344	1.9, 344
location B	3.0, 357	3.0, 357	3.0, 357
Depth of 0.75 MPa[1]:			
location A (m)	0.9	0.9	0.9
location B	2.2	2.2	2.2
Strs.- mean Δ°T at location A:			
location A (MPa,Day)	1.2, 329	1.2, 329	1.2, 329
location B	1.6, 329	1.6, 329	1.6, 329
Frost penetration:			
location A (m)	6.6	6.6	6.6
location B	5.9	5.8	5.6
Max. displacement:			
crest (mm, Day)	6, 45	7, 50	6, 50

1: On day of critical temperature gradient at location A.

When the conduction coefficient, k, is 1.87 W/(m°K), the maximum stress at location A increases by 10% and at location B by 3%. The depth of frost penetration at B decreases by 15% When the conduction coefficient, k, is 3.68 W/(m°K), the maximum stress at A is reduced by 15%, the stress at B is reduced by 7%, and the depth of frost penetration increases by 19% at location B. The depth of the 0.75 MPa is not significantly affected for both cases. The variation in specific heat has a negligible effect on the response parameters of the system.

7.4 Effects of Concrete Mechanical Properties on Dam Response

The mechanical properties of the system are never known exactly, especially for old dams where aging may affect the concrete strength and stiffness. Moreover, the dam may be under plane stress or plain strain condition depending on the state of the interface monolith joints If the monoliths of the dam act as a continuous section, the dam will be under plane strain conditions. If the monoliths are free to move independently of each other, then the dam will be under plane stress conditions. When a plane strain formulation is used, the maximum stresses increase by about 27%. The depth of the 0.75 MPa line increases by 33% at location A and by 9% at location B (table 7.4).

The foundation may provide different degrees of restraint to the base of the dam depending on the continuity condition provided by the interface friction and cohesion. Extreme dam-foundation interface continuity conditions may be simulated by using fixed and free dam restraints at the interface. As table 7.4 shows, the degree of restraint of the foundation has a negligible effect on the system away from the foundation-dam interface. When the foundation is part of the finite element model, the principal thermal tensile stresses close to the heel and

Table 7.4: Influence of structural modelling on the thermal and structural behaviour for a 45m dam.

Response Parameter	Plane Strain	Plane Stress	Foundation		
			Fixed	FEM	Free
Mean annual °T:					
complete dam (°C)	4.0	4.0	4.0	4.0	4.0
top section	4.2	4.2	4.2	4.2	4.2
mid-section	4.0	4.0	4.0	4.0	4.0
bottom section	4.1	4.1	4.1	4.1	4.1
Minimum mean °T:					
complete dam (°C,Day)	0.9, 50	0.9, 50	0.9, 50	0.9, 50	0.9, 50
top section	-4.4, 50	-4.4, 50	-4.4, 50	-4.4, 50	-4.4, 50
mid-section	0.7, 69	0.7, 69	0.7, 69	0.7, 69	0.7, 69
bottom section	2.2, 50	2.2, 50	2.2, 50	2.2, 50	2.2, 50
Critical °T gradient:					
location A (°C,Day)	-16.3, 18	-16.3, 18	-16.3, 18	-16.3, 18	-16.3, 18
location B	-15.8, 18	-15.8, 18	-15.8, 18	-15.8, 18	-15.8, 18
Maximum surface Δ°T:					
location A (°C,Day)	5.9, 344	5.9, 344	5.9, 344	5.9, 344	5.9, 344
location B	13.6, 357	13.6, 357	13.6, 357	13.6, 357	13.6, 357
Max. tensile stress :					
location A (MPa,Day)	2.4, 344	1.9, 344	1.9, 344	1.9, 344	1.9, 344
location B	3.8, 357	3.0, 357	3.1, 357	3.0, 357	3.1, 357
Depth of 0.75 MPa[1]:					
location A (m)	1.2	0.9	0.9	0.9	0.9
location B	2.4	2.2	2.2	2.2	2.2
Strs.- mean Δ°T at location A:					
location A (MPa,Day)	1.6, 329	1.2, 329	1.2, 329	1.2, 329	1.2
location B	2.1, 329	1.6, 329	1.7, 329	1.6, 329	1.7
Frost penetration:					
location A (m)	6.6	6.6	6.6	6.6	6.6
location B	5.8	5.8	5.8	5.8	5.8
Max. displacement:					
crest (mm, Day)	7, 50	7, 50	6, 50	7, 50	-

1: On day of critical temperature gradient at location A.

toe, on the day when the stress at location B is maximum, are 0.6 MPa and 2.8 MPa, respectively The principal thermal tensile stresses obtained close to the heel and toe when a fixed base is assumed are 0 5 MPa and 3.2 MPa, respectively, and when the base is on rollers the principal thermal tensile stresses are 0.4 MPa and 1.0 MPa, respectively.

Due to the long term action of stress, creep gives rise to an increase in concrete strain which relieves some of the induced temperature stresses. To take into account the effects of creep, the instantaneous modulus of elasticity, E, is reduced to an effective value, as was previously mentioned. In the current state of practice, the instantaneous modulus of elasticity is reduced from 20% to 40% (Hayward et al. 1991; Paul and Tarbox 1991; NRC 1990). Due to the effects of aging the modulus of elasticity may itself vary by approximately $\pm$20%. The modulus of elasticity is also affected by temperature. The modulus of elasticity at -10 °C is about 10% larger than when the temperature is 20 °C (Lee et al 1988). Based on these conditions, a lower (13375 MPa) and upper (29500 MPa) bound for the modulus of elasticity is obtained. Note that the effective modulus of elasticity used in the initial analysis, when creep is considered, is 18175 MPa. Since the system is assumed linear elastic, the stresses vary linearly with the variation in the modulus of elasticity. The maximum thermal tensile stresses are reduced by about 25% when the lower bound for the modulus of elasticity is used, while the maximum thermal tensile stresses increase by about 60% when the upper bound for the modulus of elasticity is used (table 7.5).

The coefficient of thermal expansion is a function of the type of aggregate. The lower and upper limits selected from the literature are 7.7×10^{-6}/°K and 10.3×10^{-6}/°K (ACI 1981). The maximum thermal tensile stresses are reduced by about 15% when the lower limit of the

Table 7.5. Influence of E and α on the thermal and structural behaviour of a 45m dam.

Response Parameter	E (MPa)			α (10^{-6}/°K)		
	13375	18175	29500	7 7	8.9	10.3
Mean annual °T:						
complete dam (°C)	4.0	4.0	4.0	4.0	4 0	4.0
top section	4.2	4.2	4.2	4.2	4 2	4.2
mid-section	4.0	4.0	4.0	4.0	4.0	4.0
bottom section	4.1	4.1	4.1	4.1	4.1	4.1
Minimum mean °T:						
complete dam (°C,Day)	0.9, 50	0.9, 50	0.9, 50	0.9, 50	0.9, 50	0.9, 50
top section	-4.4, 50	-4.4, 50	-4.4, 50	-4.4, 50	-4 4, 50	-4.4, 50
mid-section	0.7, 69	0.7, 69	0.7, 69	0.7, 69	0.7, 69	0.7, 69
bottom section	2.2, 50	2.2, 50	2.2, 50	2.2, 50	2.2, 50	2.2, 50
Critical °T gradient:						
location A (°C,Day)	-16.3, 18	-16.3, 18	-16.3, 18	-16.3, 18	-16.3, 18	-16.3, 18
location B	-15.8, 18	-15.8, 18	-15.8, 18	-15.8, 18	-15.8, 18	-15 8, 18
Maximum surface Δ°T:						
location A (°C,Day)	5.9, 344	5.9, 344	5.9, 344	5.9, 344	5.9, 344	5.9, 344
location B	13.6, 357	13.6, 357	13.6, 357	13.6, 357	13.6, 357	13.6, 357
Max. tensile stress :						
location A (MPa,Day)	1.4, 344	1.9, 344	3.0, 344	1.6, 344	1.9, 344	2.2, 344
location B	2.3, 357	3.0, 357	4.8, 357	2.6, 357	3.0, 357	3.4, 357
Depth of 0.75 MPa[1]:						
location A (m)	0.7	0.9	1.4	0.8	0.9	1.1
location B	1.8	2.2	2.6	2.0	2.2	2.3
Strs.- mean Δ°T at location A:						
location A (MPa,Day)	0.9, 329	1.2, 329	2.0, 329	1.0, 329	1.2, 329	1.4, 329
location B	1.2, 329	1.6, 329	2.6, 329	1.4, 329	1.6, 329	1.9, 329
Frost penetration:						
location A (m)	6.6	6.6	6.6	6.6	6.6	6.6
location B	5.8	5.8	5.8	5.8	5.8	5.8
Max. displacement:						
crest (mm, Day)	6, 50	7, 50	6, 50	5, 50	7, 50	7, 50

1: On day of critical temperature gradient at location A.

coefficient of thermal expansion is used, and increase by about the same amount for the upper limit.

7.5 Effects of Environmental Conditions

7.5.1 Effect of Air Temperature

The air temperature that was used in the preliminary analysis was based on a 22 year average. The averaging process has the effect of smoothing any large thermal shock that the system may experience. To investigate the effect that the averaging process has on the response of the system, actual measured air temperatures are used for the third year of the analysis. Three years are chosen; the year with the lowest mean annual temperature, the year with the lowest monthly temperature, and the year with the lowest daily temperature (fig. 7.3).

When actual air temperature variations are used, the maximum surface tensile stresses increase by a factor ranging from 1.5 to 2 (table 7.6). This large increase is due to the large temperature change that occurs from day to day. This increase in stresses is limited to the surface of the dam since the depth of the 0.75 MPa line does not vary by a large amount. Figure 7.4 shows the temperature and tensile stress envelopes for each year. The maximum depth of frost penetration occurs for the year with the coldest monthly temperature; note that the increase is only of 5%.

As was previously discussed, the air temperature may be modelled by a sinusoidal equation [5.1] (fig. 5.1b). The effects of modelling the air temperature by a sine curve are

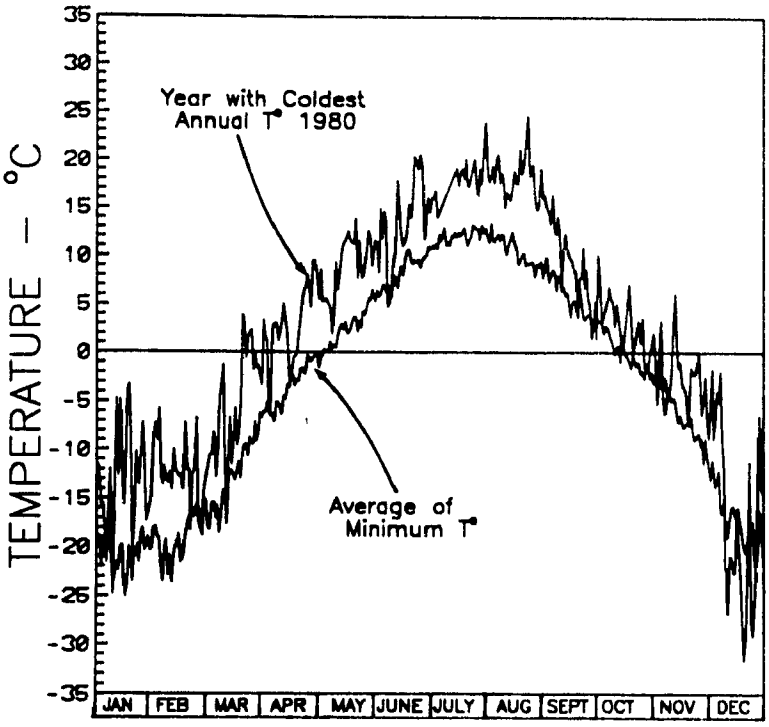

(a)

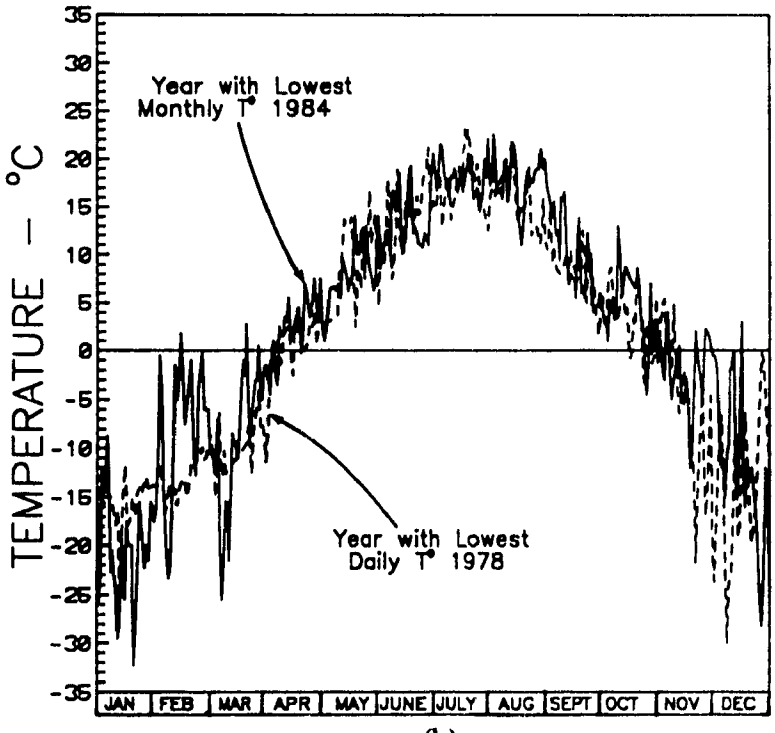

(b)

Figure 7.3 Air temperature: (a) average minimum air temperature and year with lowest annual temperature; (b) year with lowest monthly temperature and year with lowest daily temperature.

Table 7.6: Influence of air temperature on thermal and structural behaviour of a 45m dam.

Response Parameter	Year with Coldest			Average Air Temperature		
	Year (1980)	Month (1984)	Day (1978)	22 Yr	Sin	Min.
Mean annual °T:						
complete dam (°C)	4.1	4.0	3.8	4.0	3.8	1.2
top section	4.3	4.1	3.6	4.2	3.9	0.7
mid-section	4.1	3.9	3.6	4.0	3.7	1.0
bottom section	4.2	4.0	3.9	4.1	3.9	1.3
Minimum mean °T:						
complete dam (°C,Day)	0.8, 59	0.3, 41	0.8, 85	0.9, 50	0.8, 55	-2.1, 50
top section	-4.7, 361	-6.5, 22	-4.4, 50	-4.4, 50	-4.4, 41	-8.2, 50
mid-section	0.6, 59	0.0, 69	0.4, 85	0.7, 69	0.5, 62	-2.3, 70
bottom section	2.1, 59	1.8, 69	2.1, 85	2.2, 50	2.1, 59	-0.6, 70
Critical °T gradient:						
location A (°C,Day)	-27.0, 355	-27.0, 22	-24.8, 343	-16.3, 18	-13.0, 16	-22.3, 18
location B	-26.6, 356	-25.5, 22	-22.8, 344	-15.8, 18	-13.0, 16	-21.8, 19
Maximum surface Δ°T:						
location A (°C,Day)	16.0, 346	13.9, 361	15.5, 343	5.9, 344	4.0, 338	7.0, 347
location B	26.3, 356	23.4, 361	23.4, 344	13.6, 357	11.2, 354	14.5, 357
Max. tensile stress :						
location A (MPa,Day)	4.0, 346	3.7, 361	4.0, 343	1.9, 344	1.5, 338	2.1, 347
location B	5.4, 356	4.7, 361	4.7, 344	3.0, 357	2.6, 354	3.1, 357
Depth of 0.75 MPa[1]:						
location A (m)	1.0	1.2	1.2	0.9	0.9	1.8
location B	2.5	2.6	2.6	2.2	2.2	3.1
Strs.- mean Δ°T at location A:						
location A (MPa,Day)	1.9, 22	1.8, 348	2.4, 332	1.2, 329	0.8, 278	1.0, 11
location B	2.8, 22	1.8, 348	3.1, 332	1.6, 329	0.2, 278	2.3, 11
Frost penetration:						
location A (m)	6.5	6.7	6.6	6.6	6.6	6.9
location B	5.5	6.1	6.1	5.8	6.2	12.1
Max. displacement:						
crest (mm, Day)	7, 361	8, 22	6, 50	7, 50	6, 41	8, 50

1: On day of critical temperature gradient at location A.

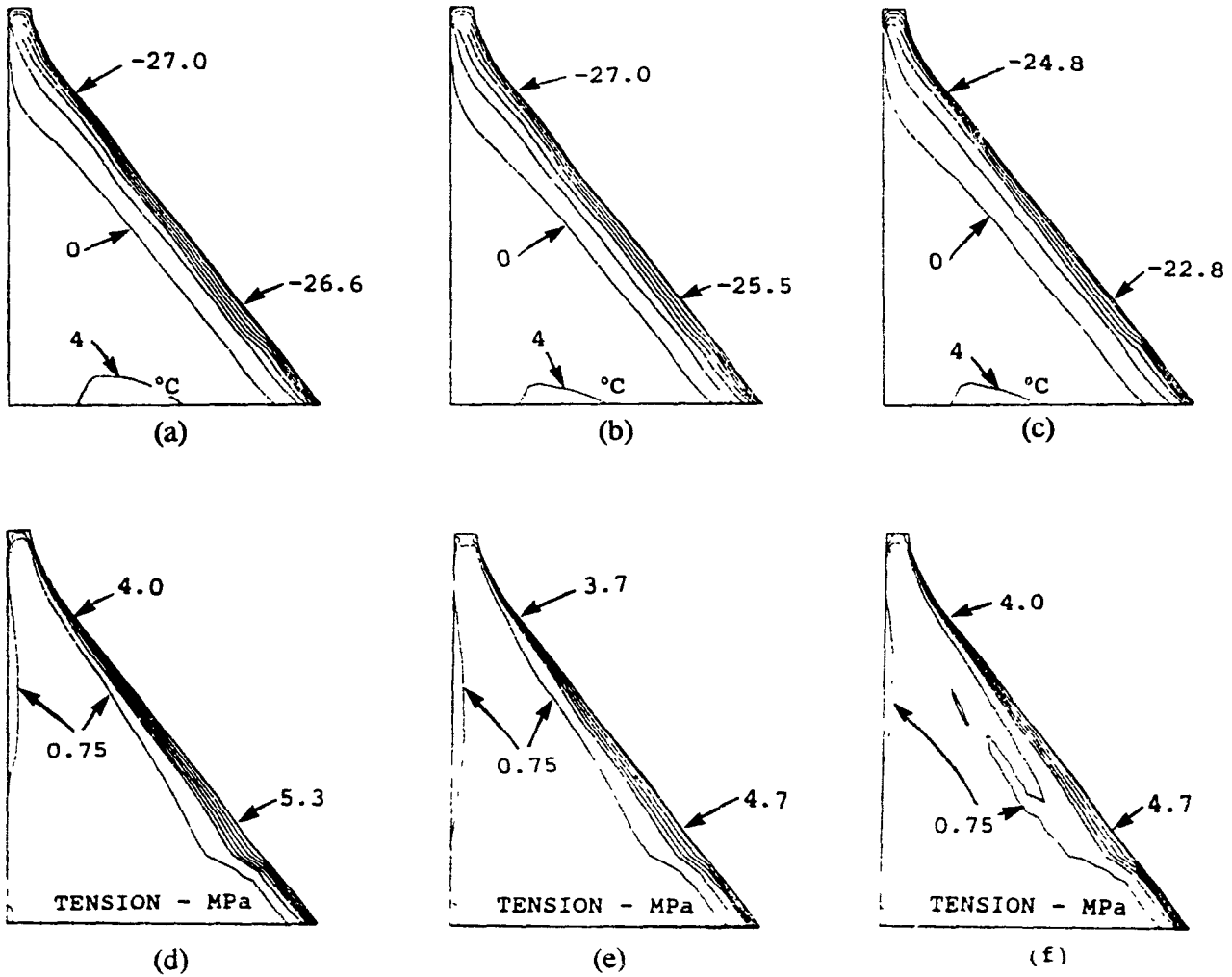

Figure 7.4 Tensile stress and temperature envelopes: (a) minimum temperature envelope for year with lowest mean annual temperature, (b) minimum temperature envelope for year with lowest monthly temperature, (c) minimum temperature envelope for year with lowest daily temperature; (d) tensile stress envelope for year with lowest annual temperature, (e) tensile stress envelope for year with lowest monthly temperature; (f) tensile stress envelope for year with lowest daily temperature.

investigated. When a sinusoidal representation is used, the maximum surface tensile stress at location A is reduced by 22%, while at B a reduction of 15% occurs. This drop is due to the uniformity of the sine curve which produces no thermal shocks. The location of the 0.75 MPa line remains unchanged. The depth of frost penetration at location B increases by 7%.

To investigate the effects of extreme air temperatures on the dam, an average of minimum recorded air temperatures over a 22 year period is used (fig 7.3). The maximum tensile stress at location A is found to increase by 10%, while at location B the increase is of 3%. The depth of the 0.75 MPa line increases by a factor of 2 at location A, and by 44% at location B. The depth of frost penetration at location B increases by a factor of 2.

7.5.2 Effect of Reservoir Temperatures

As previously discussed, 2 types of reservoirs are generally recognized. The effects of the second type of reservoir, type II (fig. 5.5b), are investigated. The maximum temperature is assumed to be 14 °C and the minimum temperature is assumed to be 0.5 °C. The transition from 0 °C to 0.5 °C is assumed to occur over a depth of 5m. The computed maximum tensile stresses at locations C and D are 1 MPa, while the stresses for the type I reservoir are 0.8 MPa and 0.6 MPa at locations C and D, respectively. The type II reservoir has a negligible effect on the thermal and stress response on the downstream face (table 7.7). Figure 7.5 shows the temperature and stress envelopes.

If the catchment area for the reservoir is small, draw down of the reservoir for power may exceed the water inflow during winter when the river flows are small. Therefore, the

Table 7.7: Influence of reservoir on thermal and structural behaviour for a 45m dam.

Response Parameter	Reservoir		
	Type II	Type I	Oper.
Mean annual °T:			
complete dam (°C)	4.7	4.0	4.7
top section	4.7	4.2	4.3
mid-section	4.7	4.0	4.7
bottom section	4.7	4.1	4.7
Minimum mean °T:			
complete dam (°C,Day)	1.1, 50	0.9, 50	1.0, 50
top section	-4.4, 50	-4.4, 50	-5.8, 44
mid-section	0.8, 69	0.7, 69	0.8, 69
bottom section	2.5, 70	2 2, 50	2.5, 70
Minimum surface °T:			
location A (°C,Day)	-16.3, 18	-16.3, 18	-16 3, 18
location B	-15.7, 18	-15.8, 18	-15.7, 18
Critical °T gradient:			
location A (°C,Day)	6.1, 344	5.9, 344	6.0, 344
location B	13.7, 357	13.6, 357	13 7, 357
Max. tensile stress :			
location A (MPa,Day)	2.0, 344	1.9, 344	2.0, 344
location B	3.0, 357	3.0, 357	3.0, 357
Depth of 0.75 MPa[1]:			
location A (m)	1.1	0.9	1.3
location B	2.2	2.2	2.2
Strs.- mean Δ°T at location A:			
location A (MPa,Day)	1.3, 6	1.2, 329	1.3, 6
location B	2.7, 6	1.6, 329	2.7, 6
Frost penetration:			
location A (m)	6.9	6.6	7.0
location B	5.5	5.8	5.5
Max. displacement:			
crest (mm, Day)	6, 50	7, 50	6, 44

1: On day of critical temperature gradient at location A.

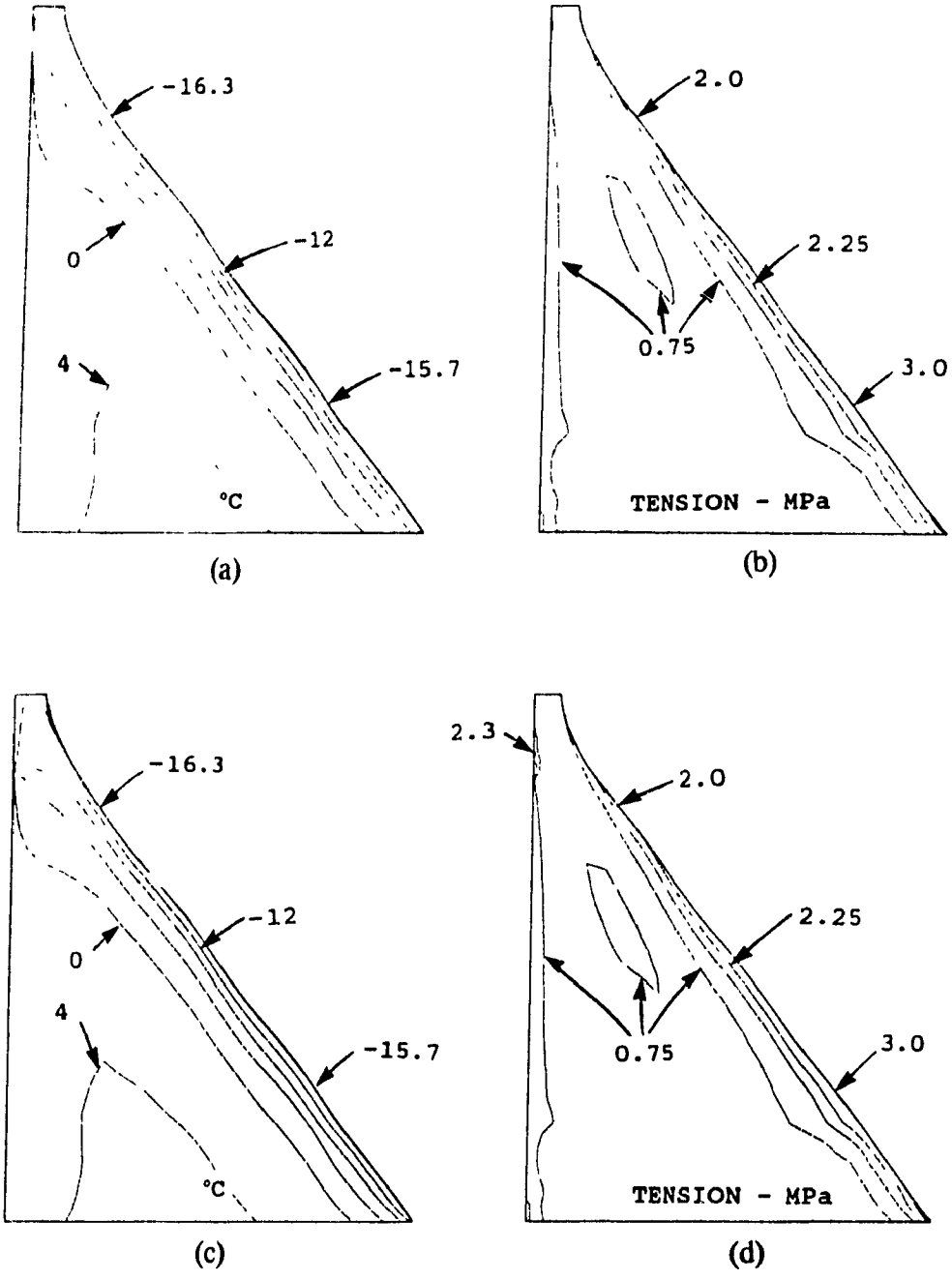

Figure 7.5 Type II reservoir: (a) temperature envelope; (b) tensile stress envelope. Operational reservoir condition: (c) temperature envelope; (d) tensile stress envelope.

upstream face of the dam may become exposed to freeze and thaw cycles for a significant portion of the dam height. This is particularly critical because near the fluctuating water surface level the concrete is in a saturated condition and very susceptible to damage induced by cyclic frost penetration. To model this operating condition, the water level is assumed to be reduced by 5m during the winter seasons (note that the effects of phase change are not considered in the transient heat flow analysis). The drop in water level is assumed to occur gradually from November 15 to December 15, and the water level is assumed to rise gradually from April 15 to May 15. The operational reservoir condition affects the depth of the 0.75 MPa line at location A, which increases by 44%. The main change is in the stresses on the upstream face of the dam (fig. 7.5). For example, the stress at a depth of 3m below the initial water surface (43m) is 2.3 MPa as compared to a value of 0.5 MPa when the reservoir level is not changing.

7.5.3 Effect of Solar Radiation

The amount of solar radiation reaching the surface of the dam depends on the absorptivity of the concrete and on the terrain factor. To simulate extreme conditions, solar radiation is first assumed not to reach the dam (terrain factor = 0) and then 65% (terrain factor = 1, a=0.65) of the solar radiation is assumed to reach the dam. Note that for a terrain factor of 0.75 and an absorptivity of 0.5, corresponding to the previous analysis, the percentage of solar radiation absorbed by the dam is 38%. Another factor affecting solar radiation is the orientation of the dam. A southern exposure will receive the highest amount of solar radiation, while a northern exposure will receive the least.

Figure 7.6 shows the surface temperature at location A when solar radiation is

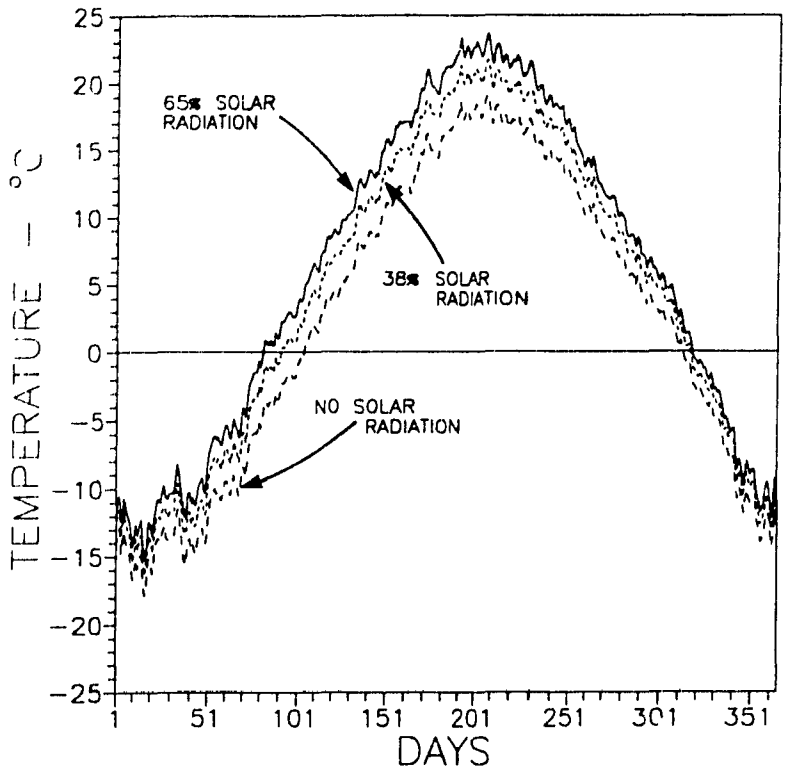

Figure 7.6 Time history of surface temperature at location A with and without solar radiation.

considered. The maximum increase in surface temperature is 3 °C and 5 °C when solar radiation is 38% and 65%, respectively, and this occurs in mid june. The smallest temperature increase is 1.2 °C and 2.0 °C and this occurs towards the end of October. The mean annual increase in temperature when 38% of the solar radiation is absorbed by the dam is 2.1 °C. The annual increase in temperature, due to solar radiation, obtained from data available from Tarbox (1977) is 4.3 °C. The data available from Tarbox (1977) therefore overestimates the temperature increase due to solar radiation.

Figure 7.7 shows the maximum and minimum temperature envelopes for each case. Solar radiation affects mainly the depth of frost penetration (table 7.8). When no solar radiation is considered, the depth of frost penetration at location B increases by 28%. When 65% of solar

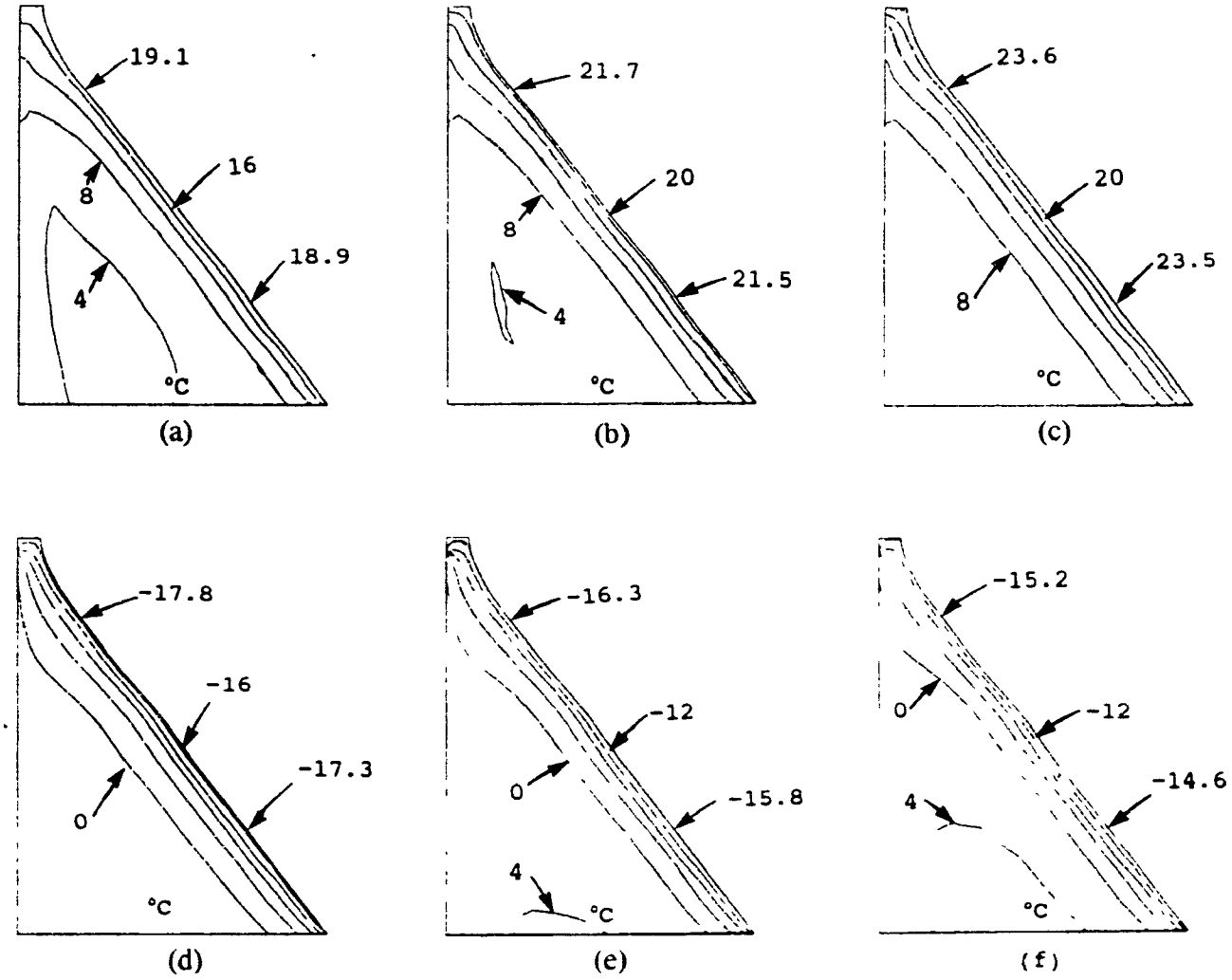

Figure 7.7 Temperature envelopes: (a) maximum temperature envelope with no solar radiation; (b) maximum temperature envelope with 38% solar radiation; (c) maximum temperature envelope with 65% solar radiation; (d) minimum temperature envelope with no solar radiation; (e) minimum temperature envelope with 38% solar radiation; (f) minimum temperature envelope with 65% solar radiation

Table 7.8: Influence of solar radiation and foundation on thermal and structural response for a 45m dam.

Response Parameter	Solar Radiation			Foundation	
	0%	38%	65%	No	Present
Mean annual °T:					
complete dam (°C)	3.1	4.0	4.8	4.0	4.0
top section	3.1	4.2	5.0	4.2	4.2
mid-section	2.9	4.0	4.8	4.0	4.0
bottom section	3.2	4.1	4.7	4.0	4.1
Minimum mean °T:					
complete dam (°C,Day)	0, 50	0.9, 50	1.5, 50	0.8, 50	0.9, 50
top section	-5.4, 50	-4.4, 50	-3.7, 44	-4.4, 50	-4 4, 50
mid-section	-0.3,69	0.7, 69	1.4, 50	0.7, 69	0.7, 69
bottom section	1.4, 70	2.2, 50	2.8, 50	2.0, 50	2.2, 50
Minimum surface °T:					
location A (°C,Day)	-17.8, 18	-16.3, 18	-15.2, 18	-16.3, 18	-16.3, 18
location B	-17.3, 19	-15.8, 18	-14.6, 18	-15.8, 18	-15.8, 18
Critical °T gradient:					
location A (°C,Day)	5.9, 344	5.9, 344	5.9, 344	5.9, 344	5.9, 344
location B	13.5, 357	13.6, 357	13.7, 357	13.6, 357	13.6, 357
Max. tensile stress :					
location A (MPa,Day)	1.8, 344	1.9, 344	1.9, 344	1.9, 344	1.9, 344
location B	2.9, 357	3.0, 357	3.0, 357	3.0, 357	3.0, 357
Depth of 0.75 MPa[1]:					
location A (m)	0.9	0.9	1.0	0.9	0.9
location B	2.2	2.2	2.2	2.2	2.2
Strs.- mean Δ°T at location A:					
location A (MPa,Day)	1.2, 329	1.2, 329	1.2, 313	1.2, 329	1.2, 329
location B	1.5, 329	1.6, 329	1.0, 313	1.6, 329	1.6, 329
Frost penetration:					
location A (m)	6.7	6.6	6.5	6.6	6.6
location B	7.4	5.8	4.8	5.8	5.8
Max. displacement:					
crest (mm, Day)	8, 50	7, 50	5, 44	7, 50	7, 50

1: On day of critical temperature gradient at location A.

radiation is absorbed by the dam the depth of frost penetration at location B decreases by 17%. The effect on the stresses is negligible.

7.5.4 Effect of Thermal Response of Foundation

The foundation is sometimes not modeled in the transient heat flow analysis. When this is done, an adiabatic condition is assumed at the dam-foundation interface. As can be seen from table 7.8 this has no effect on the response of the system away from the dam-foundation interface. The tensile thermal stress close to the heel, on the day when the stress is critical at location B, is 0.9 MPa and the stress close to the toe is 2.7 MPa. When the foundation is considered in the transient heat flow analysis, the stresses close to the heel and toe are 0.6 MPa and 2.8 MPa, respectively. Note that for the stress analysis the foundation is included in the finite element model.

7.6 Correlation with Simplified Analysis Procedures

Many empirical formulae have been developed to obtain the temperature variation in concrete dams. One such equation developed for thick concrete sections, assuming a sinusoidal representation for the air temperature, is (ACI 1981):

[7.1]
$$\frac{R_x}{R_o} = e^{-x\sqrt{\frac{\pi}{h^2 \gamma}}}$$

where

[7.2] $$h^2 = \frac{k}{c\,\rho}$$

in which R_x is the amplitude of the temperature at the location of interest, in °C; R_o is the amplitude of the surface temperature, in °C; x is the depth of the point of interest, in m; γ is the period of the air temperature, 365 days; h^2 is the diffusivity of concrete, in m^2/day; k is the conduction coefficient, in J/(day m °K); c is the specific heat of concrete, in J/(kg°K); ρ is the density of concrete, in kg/m^3. From equation [7.1], the amplitude at a depth of 0.8m from location A is 13.0 °C. Note that the amplitude of the average air temperature distribution is 16.5 °C. For the 45m dam subjected to the average air temperature distribution the amplitude obtained from the finite element transient heat flow analysis at a depth of 0.8m is 14.5 °C. The amplitude obtained from the transient heat flow analysis is 10% larger than that obtained from equation [7.1].

The time lag, Z, which is the length of time for which changes in external temperature take to penetrate to a point x, may be approximated from:

[7.3] $$Z = \frac{A}{h^2}$$

where A is the cross sectional area to reach the point x, in m^2. From equation [7.3] a time lag of 8 days is obtained. The time lag obtained from the transient heat flow analysis is 11 days (fig. 7.8). The results obtained from equations [7.1] and [7.3] and from the finite element transient heat flow analysis are found to be in good agreement. The critical temperature gradient obtained from equations [7.1] and [7.3] is 5.5 °C. The temperature gradient is obtained from a sinusoidal representation of the air temperature, since equation [7.1] is based on this

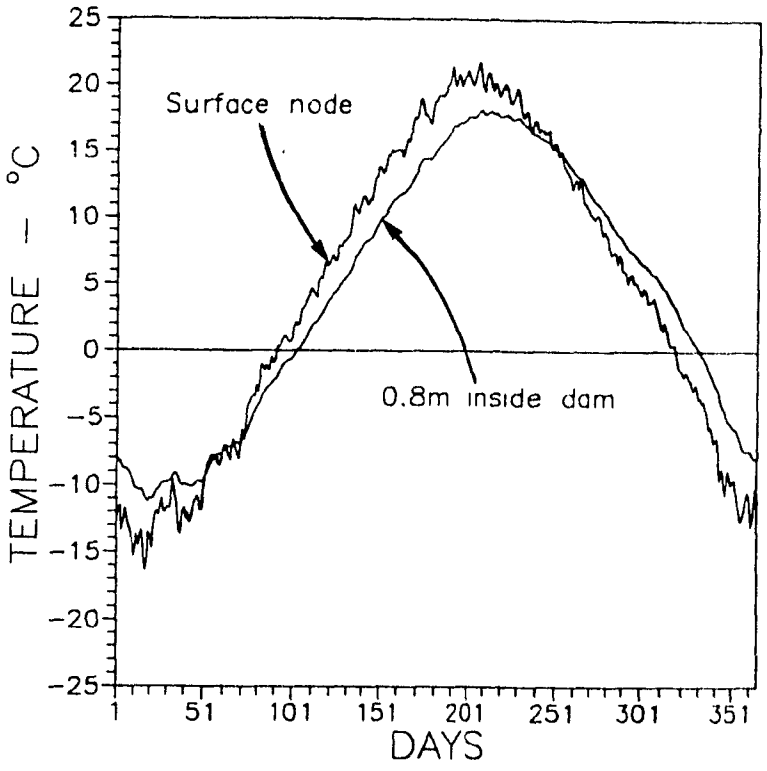

Figure 7.8 Temperature at location A and at a depth of 0.8m from location A.

assumption. The critical temperature gradient obtained from the finite element transient heat flow analysis is 5.9 °C, which is 7% larger than that obtained from equation [7.1] and [7.3].

Assuming a fully restrained condition, the stress may be obtained from:

[7.4] $$\sigma_T = E_{eff}\ \alpha\ \Delta T$$

where E_{eff} is the effective modulus of elasticity, in MPa. The stress obtained from equation [7.4] is 0.9 MPa and represents an average value for the area from the surface to a depth of 0.8m. The average stress obtained from the finite element analysis over the same depth is 1.4 MPa. The amplitude and phase shift at location A are accurately predicted by equations [7.1]-[7.3], but the average stress is underestimated by equation [7.4].

As a simplified procedure, one may think that a steady state analysis using external temperature conditions corresponding to a critical state might be performed to obtain critical thermal and stress distributions. However, a steady state analysis will produce unrealistic temperature gradients and corresponding stresses. For example, when a steady state analysis is performed for the 45m dam, on the day when the temperature gradient is critical at location A (based on an average air temperature distribution) the surface stresses are of the order 0.2 MPa, and the frost penetration at location B is 20.4m. Therefore, the transient nature of the thermo-mechanical response must be considered to obtain realistic results.

CHAPTER 8

Summary and Conclusions

8.1 Summary

Dam safety evaluation requires a realistic definition of all loads that influence the structural behaviour of the dam-foundation-reservoir system. For dams built in northern regions, seasonal thermal stresses contribute significantly to the final stress condition in the vicinity of the downstream face. Repeated freeze-thaw cycles and related frost penetration also contribute significantly to strength and stiffness degradation. Thermal stresses have often been estimated using simplified assumptions with crude analysis procedures. Seasonal temperature and stress distributions may be obtained in a more rigorous manner by using finite element transient heat flow analysis in conjunction with stress analysis. The results are necessary to optimize the rehabilitation of existing dams through thermal insulation (eg. Daniel Johnson) or restraint releases by the introduction of joints (eg. Paugan, Fontana). Realistic thermal stresses and strains are also required to perform reliable fracture and seismic safety analyses. Moreover, auscultation and surveillance of dams rely on measurements of deformations, strains, water leakage, and uplift pressure. To asses the structural integrity of the dam, the reversible part of each measured quantity due to hydrostatic and seasonal temperature variations must be determined to evaluate the irreversible part of the deformations.

This study presented a methodology to compute seasonal temperature and stress distributions in concrete gravity dams by using a finite element technology operational on microcomputers and widely available in the industry. An extensive parametric analysis was performed to investigate the effects of different modelling assumptions related to the geometric, thermal, and mechanical properties of the dam, and the influence of external heat fluxes supplied by the air, sun, reservoir, and foundation, on the thermo-mechanical response of the system.

8.2 Conclusions

Seasonal variations of temperatures provide significant tensile stressing mechanisms in the vicinity of the downstream face during cold temperature periods. Based on the procedures developed, and the numerical investigations reported, the following conclusions may be drawn:

(1) To obtain a rapid convergence of the cyclical thermal behaviour of the dam-foundation-reservoir system, when seasonal thermal variations are present at the boundaries of the system, the initial temperature distribution must be near to the mean annual temperature distribution of the dam. The temperature distribution obtained from a steady state analysis gives a reliable estimate of the mean temperature distribution of the system when yearly average temperatures are applied at the boundaries of the system.

(2) Maximum surface tensile stresses occur when the temperature gradient between the surface node and the first inside node is greatest (critical gradient). This does not hold true for any pair of inside nodes. "Mean" surface tensile stresses, corresponding to approximately half of the maximum critical tensile stresses, occur when the temperature gradient between the surface node

and a node located at a depth of about 1m from the surface of the dam, is half that of the critical gradient.

High temperature gradients are limited to about a depth of 5m from the air exposed face of the dam. High tensile thermal stresses are limited to the face of the dam. For the 90m dam examined in this study, the maximum thermal tensile stress at a point located in the top third of the dam is 2.7 MPa, and the depth of the 0.75 MPa line is 2m. The stresses at the same location for the 45m and 22.5m dams analyzed in this study are 1.9 MPa and 0.9 MPa, respectively, and the depths of the 0.75 MPa line are 0.9m and 0.1m, respectively.

Thermal tensile stresses may produce surface cracking that will not affect the structural resistance of the dam significantly, however, these surface cracks may be very detrimental to the long term serviceability of the dam. Water penetration, coupled with repeated freeze-thaw cycles, has been found to produce severe deteriorations in dams built in northern regions. In extreme cases the structural integrity of the dam-foundation-reservoir system may be threatened. The location of high thermal stresses in the top region of the dam corresponds to the region where seismic induced cracking is likely to occur. Thus, initial thermal tensile stresses should be considered in a comprehensive seismic safety analysis since they may affect crack initiation and propagation.

(3) The height of the dam has little effect on the depth of frost penetration, of the order of 6m, and on the spatial distribution of the thermal field. However, height affects the stiffness and structural response. As the dam height decreases, so do the thermal stresses. The maximum thermal tensile stresses at a point located in the upper third of the dams are 2.7 MPa, 1.9 MPa,

and 0.9 MPa for the 90m, 45m, and 22.5m dams analyzed in this study, respectively.

(4) Maximum crest displacements occur when the mean temperature of the upper third section of the dam is lowest. A very good approximation (within 2%) of the maximum crest displacement may be obtained from a structural analysis carried out on the day when the mean temperature of the complete dam is lowest. The maximum crest displacements obtained during the cold and warm periods are close to each other. Values of 10mm, 7mm, and 5mm are respectively obtained for the 90m, 45m, and 22.5m dams subjected to average daily air temperature variations.

(5). The main concrete thermal properties used in the transient heat flow analysis are the convection coefficient, h_c, which regulates the heat exchange between air and concrete, and the conduction coefficient, k, and specific heat, c, which are strongly influenced by the type of concrete aggregate. The convection coefficient affects mainly the thermal response of the dam. When the convection coefficient is based on the assumption that no wind is present, the depth of frost penetration at a point located in the bottom third of the dam decreases by 38% as compared to the case when the convection coefficient is based on an average wind speed. When the convection coefficient is 75% larger than the value obtained from an average wind speed, the depth of frost penetration increases by 10%. The conduction coefficient, k, affects both the thermal and structural response. Analysis with conduction coefficients of 1.87 W/(m°K), 2.62 W/(m°K), and 3.68 W/(m°K) were conducted for the 45m dam. When the lower bound value is used, the stresses increase by 3% to 10% with respect to when a value of 2.62 W/(m°K) is used, and the depth of frost penetration at a point located in the bottom third of the dam decreases by 15%. When the upper bound value is used, the stresses are reduced by 7% to

15%, and the depth of frost penetration increases by 19%. The specific heat coefficient, c, has a negligible effect on the thermal and structural response of the system.

(6) Continuity conditions along the longitudinal axis have a significant effect on the seasonal thermal stresses. If the monoliths of the dam act as a continuous section, the dam may be considered to be under plane strain conditions. When the monoliths act independently of each other the dam may be considered to be under plane stress conditions. A plane strain formulation causes the maximum thermal tensile stresses to increase by 27% with respect to when a plane stress condition is used. It should be noted that the plane stress material properties (E, ν, α) of quadrilateral elements can be modified as follows to produce a plane strain condition:

[8.1] $$E_{pstrain} = \frac{E}{(1 - \nu^2)}$$

[8.2] $$\nu_{pstrain} = \frac{\nu}{(1 - \nu)}$$

[8.3] $$\alpha_{pstrain} = \alpha\ (1 + \nu).$$

Considering $\nu = 0.2$, stress increases of the order of 25% for plane strain condition can be expected from the increased material properties over the plane stress formulation.

The continuity provided at the dam-foundation interface by friction and cohesion has a negligible effect on the thermo-mechanical response of the system away from the dam-foundation interface. Near the dam foundation interface the principal tensile thermal stresses close to the toe of the dam, when the thermal gradient is critical in the bottom third of the dam, are 3.2 MPa, 2.8 MPa, and 1.0 MPa when the dam is assumed to be fixed, on a finite element foundation, and on rollers, respectively.

The foundation is sometimes not modeled in the transient heat flow analysis. When this is done, an adiabatic condition is assumed at the dam-foundation interface. The effects of this assumption away from the dam-foundation interface are negligible. The principal thermal tensile stress near the toe of the dam, when the thermal gradient is critical for the bottom third of the dam, is 2.7 MPa when the foundation is excluded from the heat flow analysis and 2.8 MPa when the foundation is considered in the transient heat flow analysis. Note that the foundation is included for the stress computations in order to obtain proper structural dam-foundation continuity condition.

The effective modulus of elasticity is a function of concrete quality, creep, age, and temperature. Based on various assumptions for concrete quality, creep, age, and temperature, the stresses obtained may decrease by 25% or increase by 60%. The coefficient of thermal expansion is a function of the concrete aggregate. The coefficient of thermal expansion may vary by $\pm 15\%$ and affect the stresses correspondingly.

(7) The daily air temperature distribution used greatly affects the surface thermal tensile stresses. When critical daily air temperature distributions are used, the maximum surface tensile stresses increase by a factor ranging from 1.5 to 2 as compared to when a daily average air temperature distribution computed from a 22 year period is used. Therefore, if "mean" thermal tensile stresses are needed an average daily air temperature distribution computed over a long period of time should be used. When air temperature distributions are not available for a site, the air temperature may be modeled as a sinusoidal distribution. A sinusoidal representation of the air temperature distribution reduces the maximum surface tensile stresses by 15% to 22% as compared to when an average daily air temperature is used. The reduction is due to the

smoothness of the sinusoidal curve which eliminates thermal shocks. If a long term average daily **minimum** air temperature distribution is used, the increase in stresses is from 3% to 10% with respect to when a long term average air temperature distribution is used, and the depth of the 0 75 MPa line and frost penetration line increase by a factor of about 2.

(8) The amount of solar radiation absorbed by the dam depends on the terrain surrounding the dam and on the absorptivity of concrete. In this study, the solar radiation absorbed by the 45m dam was assumed to be 0%, 38%, and 65%, with 38% representing an average value. When no solar radiation is assumed to reach the dam, the depth of frost penetration, at a point located in the bottom third section of the dam, increases by 28% as compared to when 38% of the solar radiation is absorbed by the dam. When 65% of the solar radiation is absorbed by the dam, the depth of frost penetration decreases by 17%. The mean annual surface temperature increase, when 38% of solar radiation is absorbed by the dam, is 2.1 °C as compared to 4.3 °C when handbook data is used (Tarbox 1977). The effect of solar radiation on stresses is negligible.

(9) The presence of the reservoir insulates the upstream face of the dam, and thus prevents the development of large thermal gradients and associated stresses in the vicinity of the upstream face. The maximum thermal tensile stresses obtained on the upstream face of the 45m dam when a reservoir with a small water intake with respect to its volume is present are of the order of 0.6 MPa to 0.8 MPa. The stresses obtained when a reservoir with an important inflow of water with respect to its volume is present are in the order of 1 MPa. If the draw down of the reservoir exceeds the inflow of water during winter conditions, the water level will fluctuate. This causes the upstream face to be exposed to large thermal shocks and the thermal tensile stresses may reach values of the order of 2.3 MPa.

(10) Empirical formulae, developed for thick concrete sections subjected to sinusoidal air temperature variations on one face, give a good indication of the amplitude and phase shift of the temperature distribution of an inside point, but for the system analyzed the average stresses obtained are underestimated.

8.3 Suggestions for Future Work

Reliable estimates of cyclical tensile stresses are needed to perform thorough safety analysis and to optimize the rehabilitation of existing dams and to ensure proper long term serviceability condition. Further work should be pursued in the following areas:

(1) Correlation of the magnitude and spatial distribution of the thermal field obtained from finite element heat transfer analysis with field temperature measurements.

(2) More time history data from dam sites should be collected and analyzed to provide a better definition of the critical temperature distributions of the climatic conditions and reservoir temperatures.

(3) A three dimensional finite element investigation of polygonal dam construction should be performed, since changes of dam orientation may affect the thermal stress distribution in the dam.

(4) A coupled thermo-mechanical analysis, with evaluation of temperature stresses considering creep in time and potential crack initiation and propagation should be performed for different

scenarios. For example, a seismic analysis coupled with a thermal analysis should be performed to determine the effect of initial thermal tensile stresses on the structural response of the system.

(5) The effects of damaged concrete on the thermo-mechanical response of the system should be investigated. Damaged concrete may result in lower thermal tensile stresses since cracks will provide a relief mechanism for the strains. However, damage induced stress redistribution may be critical for the safety of the structure.

(6) The mechanics of frost induced concrete damage should be investigated (Krali et al. 1991)

(7) The effect of change in phase of water in saturated concrete on the thermal response of the dam should be investigated. This is especially important on the upstream face of the dam where the concrete is saturated with water and where the reservoir level may fluctuate during winter conditions, thus exposing the concrete to significant thermal gradients.

(8) Procedures to provide optimal protection against water and frost penetration should be investigated (Gore and Bickley 1987; Robinsky and Bespflug 1973). Insulation methods may be active, passive, or a combination of both. Active insulation includes heating of the downstream face and passive insulation consists of protecting the downstream face with insulating materials.

(9) Procedures to repair and protect frost damaged concrete should be investigated (Barfoot 1989). It is important to prevent water from entering damaged concrete and thus causing additional damage. A method to prevent water from entering surface cracks is to apply a protective coating over the damaged area.

(10) Time series analyses of environmental data should be performed to define usual, unusual, and extreme temperature conditions in rigorous probabilistic terms.

(11) Several analyses and observations of dams located at different sites with different geometries, orientations, climatic conditions, and material properties should be performed to build a comprehensive database on the effect of the seasonal variation of temperature and thermal tensile stresses on the structural behaviour of the dam-foundation-reservoir system.

References

Abraham, T. J., and Sloan, R. C. 1978. TVA cuts deep slot in dam, ends cracking problem. ASCE, Civil Engineering, January 1978. p. 67-70.

ACI. 1981. Manual of concrete practice, part 1. American Concrete Institute, Detroit, Michigan

ASHRAE. 1982. ASHRAE handbook, 1982 applications. American Society of Heating, Refrigerating and Air-Conditioning Engineering, Inc., Atlanta. Chap. 11.

ASHRAE. 1985. Ashrae handbook, 1985 fundamentals. American Society of Heating, Refrigerating and Air-Conditioning Engineering, Inc, Atlanta. Chap. 23.

Ballivy, G , Benmokrane, B., and Chaallal, O. 1991. Déformations générées dans les bétons sous l'influence des conditions climatiques. Canadian Journal of Civil Engineering, **18**:1088-1092.

Barfoot, J. 1989. Freeze-thaw repairs to Haweswater Dam. Concrete 23:10: 44-45.

Bathe, K. J. 1982. Finite element procedures in engineering analysis. Prentice-Hall, Inc., Englewood Cliffs, New Jersey.

Baylosis, R. B. 1988. Probabilistic structural reliability study of concrete gravity dam. Ph.D dissertation. The University of Tennessee.

Bhattacharjee , S. S., and Léger, P. 1992. Concrete constitutive models for nonlinear seismic analysis of gravity dams state-of-the-art. To be published in Canadian Journal of Civil Engineering, June 1992.

Bofang, Z., and Zhanmei, L. 1990. Thermal stresses. In, Arch Dams, Ed. Laginha Serafim, J., and Clough, R. W.. A. A. Balkema, Rotterdam, Netherlands.

Cervera, M., Oliver, J., Herrero, E., and Onata, E. 1990. A computational model for progressive cracking in large dams due to the swelling of concrete. Engineering Fracture Mechanics, **35**(1/2/3): 573-585.

Cook, R. D., Walkus, D. S., and Plesha, M. E. 1989. Concepts and applications of finite element analysis. John Wiley & Sons, Inc., United States.

Dascal, O. 1991. Keeping dams safe in earthquake country. Hydro Review, August:48-55.

Dascal, O. 1990. Seismic safety evaluation of Hydro-Quebec's dams. Proceedings of 1990 Canadian Dam Safety Conference. BiTech Publishers Ltd, Vancouver, Canada. pp. 95-112

Dilger, W. H., Ghali, W., Chan, M., Cheung, M. S., and Males, M. A. 1983 Temperature stresses in composite box girder bridges. ASCE, Journal of Structural Engineering, **109**(6):1460-1478.

Duffie, J. A., and Beckman, W. A. 1980. Solar Engineering of thermal processes John Wiley and Sons, New York, NY.

Dungar, R. 1991. Bounded safety evaluation and its application for seismic loading of arch dams. Dam Engineering, 2(2): 147-161.

Elbadry, M. M., and Ghali,A. 1983. Temperature variations in concrete bridges ASCE, Journal of Structural Engineering, **109**(10):2355-2374.

Environment Canada, Atmospheric Environment Service 1985. Principal station data - Baie Comeau Minister of Supply and Services Canada. Catalogue No. En57-25/133-1985.

Environment Canada, Atmospheric Environment Service 1984. Canadian climate normals 1951 - 1980. Volume 9. Minister of Supply and Services Canada Catalogue No. En56-60/9-1984

Fanelli, M. A., and Giuseppetti, G. 1985. Numerical analysis of the thermal state of a dam. Numerical Methods in Thermal Problems, Proceedings of the Fourth International Conference Pineridge Press, Swansea, Wales, 2: 1283-1317.

Freedman, S. 1974. Properties of materials for reinforced concrete. In, Handbook of Concrete Engineering, Ed. Fintel, M.. Van Nostrand Reinhold Company, New York. Chap. 6

Gallico, A., and Cavalli, L. 1985. Les fissures de surface. Comission International des Grands Barrages, Quinzième Congrès des Grands Barrages, Lausanne. pp.571-581

Ghali, A., and Favre R. 1986. Concrete Structures: Stresses and Deformations. Chapman and Hall Ltd, New York, NY.

Geinats, G. S., Khrapkov, A. A., and Gotlif, A. A. 1989. An express method for estimating the depth of construction joint opening at the downstream face of massive concrete dams. International Symposium on Analytical Evaluation of Dam Related Safety Problems. Copenhagen, 1: 80-87.

Gore, W. and Bickley, J.A. 1987. Investigation and rehabilitation of a severely deteriorated concrete gravity structure. Concrete International, June 1987: 32-38.

Gupta, H. K. 1980. Geothermal Resources. Elsevier Scientific Publishing Company, Amsterdam, The Netherlands.

Hammer, T. A., Ryan, W. L., and Zirjacks, W. L. 1985. Ground temperature observations. In, Thermal Design Considerations in Frozen Ground Engineering. Ed. Krzewinski, T. G. and Tart, R. G. American Society of Civil Engineers. pp. 8-52.

Hayward, D. G., Thompson, G. A , Charlwood, R. G., and Steele, R. R. 1991. Remedial measures at the Mactaquac generating station Dix Septième Congrès des Grands Barrages, Vienne ICOLD, Q65 R47. pp 847-865

ICOLD. 1984. Deterioration of Dams and Reservoirs, examples and their analysis. A. A. Balkema Publishers, Boorkfield, Vermont, USA.

Ishikawa, M 1991. Thermal stress analysis of a concrete dam. Computers and Structures, **40**(2):347-352.

Jacobs, T. L. 1988. Multiobjective rehabilitation strategies for dams. Ph.D Thesis, Purdue University.

Jofriet, J. C., Jiang, S., and Tang, S. W. 1990. Finite element prediction of temperature gradients in walls of cylindrical concrete storage structures. Canadian Journal of Civil Engineering, **18**:12-19.

Kalkani, E.C. 1992. Ambient temperature effect in concrete dam foundation seepage. Journal of Geotechnical Engineering, ASCE, 118:1-11.

Krali, B., Pande, G.N. and Middeleton, J. 1991. On the mechanics of frost damage to brick masonry. Computers and Structures, 41:1:53-71.

Kreith, F., and Kreider, J. F. 1981. Principles of thermodynamics and heat transfer applied to solar energy. In, Solar Energy Handbook, Ed. Robinson, J., and Fahey, G. McGraw-Hill, United States. Chap 4.

Lee, G.C., Shih, T.S. and Chang, K.C. 1988. Mechanical properties of concrete at low temperature. Journal of Cold Regions Engineering, 2(1):13-24.

Leliavsky, S. 1981. Design textbooks in civil engineering: Volume 4, Dams. Chapman and Hall, London New York.

MacGregor, J. G., Saatcioglu, M., and Cumming, S. 1985. General. In, Concrete design handbook. Canadian Portland Association, Ottawa. Chap. 1 in Part II.

Machida, N., and Uehara, K. 1987. Nonlinear thermal stress analysis of a massive concrete structure. Computers & Structures, **26**(1/2): 287-296.

Marcotte, N., Quach, T.T., Aubin, L. et Dussault, J.G. 1977. Régime thermique des écoulements dans les régions nordiques. Compte-rendu, Troisième conférence nationale d'hydrotechnique, Société Canadienne de Génie Civil, Québec, 30 et 31 mai. pp. 616-635.

Mckay, D. C., and Morris, R. J. 1985. Solar radiation data analyses for Canada 1967-1976. Environment Canada, Atmospheric Environment Service. A publication of the Canadian Climate Program. Volume 2:Quebec. Catalogue No. EN56-64/2-1984.

Mirambell, E , and Aguado, A 1989 Temperature and stress distributions in concrete box girder bridges. ASCE, Journal of Structural Engineering, **116**(9). 2388-2409

Mlakar, P F 1987 Nonlinear response of concrete gravity dams to strong earthquake-induced ground motion Computers and Structures, **26**(1/2) 165-173

Norman, C D , and Anderson, F. A 1985 Reanalysis of cracking in large concrete dams in the US army corps of engineers. Quinzième Congrès des Grands Barrages, Lausanne. pp 157-171.

NRC, 1990 Earthquake engineering for concrete dams. Design, performance, and research needs. National Academy Press, Washington, D C .

Paul, J. W., and Tarbox, G. S 1991 Definition of critical thermal states in arch dams a prerequisite for cracking analysis Dam Fracture Proceedings from the International Conference Boulder, Colorado USA pp. 643-657.

Polivka, R. M., and Wilson, E L 1976. Dot/detect finite element analysis of nonlinear heat transfer problems. Department of Civil Engineering, University of California, Berkley, California. Report No UCB/SESM-76/2

Raphael, J. M. 1984. Tensile strength of concrete. Journal of the American Concrete Institute, **81**(2):158-165.

Robinsky, E.I. and Bespflug, K E. 1973. Design of insulated foundations Journal of the Soil Mechanics and Foundation Division, ASCE, 99· SM9: 649-667.

Rosanov, N. S., Maltsov, K. A., Plyat, C. N., and Khrapkov, A. A. 1970. Etudes du régime thermique et de l'état de contraintes thermique des grands barrages en béton Dixième Congrès des Grands Barrages, Montreal. pp. 83-93.

Sadouki, H., and Wittmann, F. H. 1991. Prediction of thermal and hygral gradients in concrete dams. Dam Engineering, **2**(1)· 21-35.

SAP90 1990. Heat transfer analysis users manual. Computers and Structures Inc, Berkeley, California

SAP90 1989. Users manual. Computers and Structures Inc, Berkeley, California.

Tahmazian, B., Yeh, C. H., and Paul, W J. 1989. Thermal cracking and arch action in Daniel Johnson dam. International Symposium on Analytical Evaluation of Dam Related Safety Problems Copenhagen, **1**: 235-244.

Tarbox, G. S. 1977. Design of concrete dams. In, Handbook of Dam Engineering. Ed. Golzé, A. R.. Van Nostrand Reinhold Company, Toronto.

Truman, K Z., Petruska, D. J , and Norman, C D 1991 Creep, shrinkage, and thermal effects on mass concrete structure ASCE, Journal of Engineering Mechanics, **117**(6): 1274-1288

Truman, K Z , Petruska, D J., Ferhi, A , and Fehl, B. 1991 Nonlinear, incremental analysis of mass-concrete lock monolith. ASCE, Journal of Structural Engineering, **117**(6): 1834-1851.

USBR, 1987 Design of small dams. Third edition, U.S. Bureau of Reclamation, Denver, Colorado

USBR, 1977. Design criteria for concrete arch dams and gravity dams Revised reprint 1977, U S Bureau of Reclamation, Monograph 19, Denver, Colorado

USBR, 1977 Design of arch dams. U S. Bureau of Reclamation, Denver, Colorado.

Veltrop, J A , Yeh, C H , and Paul, W J. 1990. Evaluation of cracks in a multiple arch dam. Dam Engineering, **1**(1): 5-12.

Widmann, R 1990 Fracture mechanics and its limits of application in the field of dam construction Engineering Fracture Mechanics, **35**(3): 531-539.